Journal of Hazardous Materials, 16 (1987) 103–138
Elsevier Science Publishers B.V., Amsterdam — Printed in The Netherlands

OVERALL PROPERTIES OF THE HEAVY GAS CLOUDS IN THE THORNEY ISLAND PHASE II TRIALS

P.W.M. BRIGHTON and A.J. PRINCE

Safety and Reliability Directorate, UKAEA, Wigshaw Lane, Culcheth, Warrington, Cheshire WA3 4NE (Great Britain)

(Received October 29, 1986; accepted January 6, 1987)

Summary

Estimation of cloud areas, advection speeds, mean ground-level concentrations and height-scales has been carried out for three flat-ground trials and all the Phase II trials, using methods previously applied to Trials 7–19. This involves visual analysis of overhead photographs; correlation of gas arrival and departure times with a simple model of the evolution of the cloud outline; calculation of average concentrations over the horizontal extent of the cloud outline; and fitting of a Gaussian profile to the resultant mean concentration profile. For Trials 20–25 this analysis was carried out separately for the portions of the cloud upwind and downwind of the barrier. Concentration results are compared with a correlation based on Trials 7–19, or with flat-ground trials at similar initial Richardson number. Local concentrations near the 9 m cubical 'building' are also compared with mean ground-level concentrations.

1. Introduction

1.1 Scope and objectives

At the first Thorney Island Syposium, we presented the results of an analysis of the area, translational speed and mean ground-level concentration of the heavy-gas clouds in Trials 7–19 of Phase I [1–4]. Cloud heights and Richardson numbers were also obtained and an overall mass balance calculated. The main objective of this work was to obtain the quantities needed for comparison with integral models of dispersion, which predict only overall cloud properties and not concentrations at individual points as measured in the experiments. Moreover, by plotting these results in dimensionless form it was possible to gauge the consistency of results from trial to trial, and to corroborate some of the basic physical assumptions underlying the integral models.

Subsequently, Wheatley et al. [5–7] have used these values of cloud properties to quantify the parameters in simple models of the dilution process and of the translational motion of the clouds.

In this paper the basic analysis of overall properties is extended to the remaining flat-ground trials (5, 6 and 34), and, with suitable modifications, to

0304-3894/87/$03.50 © 1987 Elsevier Science Publishers B.V.

the trials with a cubical obstruction (26–29), and to those with various types of semi-circular barrier (20–25).

The objectives of the Phase II trials were rather different from those of Phase I: instead of providing data for comparison with mathematical models over a wide range of conditions, a limited selection of configurations was tested to provide information for checking wind-tunnel simulations. Our analysis of overall properties is intended to help make sense of a large amount of complex data, rather than to test particular models. Nevertheless, relatively simple mathematial models for the effects of obstacles are starting to be formulated [8,9] and some qualitative comparisons can be made.

The results from the trials with the cube can possibly be regarded effectively as an additional contribution to the flat-ground data for testing integral models, since the obstacle is very small compared to the overall dimensions of the cloud. However, we also present some results on how concentrations near the building are perturbed from the mean.

1.2 Conditions in the trials

Table 1 summarises conditions in the trials considered in this paper. As in Table 1 of [2], the initial Richardson numbers are based on values of the rms vertical wind component at height 10 m, as listed in the "hard-copy" volumes of results [10]. (The value for Trial 5 given in [2] was wrong, because the effective release volume was less than that in the container initially, the release mechanism having jammed one-third of the way down.) The trials with obstacles have values of Ri_0 spanning practically the whole range achieved in Phase I. Trial 34 was specifically commissioned by the Gas Research Institute to provide data at as high a Richardson number as possible, for comparison with laboratory still-air experiments [11].

In Table 1, t_1 is the effective origin of time in the linear increase-rate law for cloud area, as in eqn. (7) of [2]. For the Phase I trials it was determined from the overhead visual records [3], but the time origin in these was uncertain by a second or two. For Trial 34 and the Phase II trials, t_1 was assumed proportional to the timescale for area increase $\mathscr{T}$, defined by

$$\mathscr{T} = R_0/2K\,(g\Delta_0' h_0)^{1/2} \tag{1}$$

where R_0 is the initial cloud radius (7 m), K is the empirical frontal Froude number (with value 1.07), g is the acceleration due to gravity, Δ_0' the initial relative density difference and h_0 the initial height. The coefficient of proportionality was determined from Spicer and Havens' [11] experiments as follows. Using a plot of radius squared R^2 against time t determined from their concentration records in Fig. 7 of [11] gave $t_1 = 15\ \mathscr{T}$. Adjusting the time origin in their own logarithmic plot of R^2 against t (Fig. 10 [11]) to get the data on the asymptotic straight line gave $t_1 = 13\ \mathscr{T}$. Hence we assumed

TABLE 1

Initial Richardson numbers, time-scales and extent of concentration measurements

Trial no.	Ri_0	t_1 (s)	τ (s)	Max no. of masts in cloud	Duration of concentration measurements (s)
(a) Flat-ground trials					
34	1.94×10^4	4.35	0.310	26	1190
6	993	3	0.421	9	464
5	260	0	0.427	4	229
(b) Building trials					
27	8.23×10^3	2.46	0.176	16	290
26	1.67×10^3	4.09	0.292	32	726
29	965	4.11	0.293	16	260
28	334	4.22	0.301	17	227
(c) Barrier trials (*denotes permeable barrier)					
25	5.28×10^3	4.16	0.297	10	755
22	2.23×10^3	2.71	0.194	20	>600
21	1.80×10^3	3.97	0.283	24	>600
24*	574	4.07	0.291	16	362
23*	535	4.40	0.314	18	362
20	500	4.32	0.308	15	252

$$t_1 = 14\ \mathscr{T}. \tag{2}$$

As seen in Table 1 this gives values around 4 s, quite consistent with the approximate values from the visual records of Phase I. As in [2], these values of t_1 were subtracted from time after release in order to form the dimensionless time used for plotting the concentration results in this paper:

$$\tau = (t - t_1)/\tau. \tag{3}$$

Table 1 also contains indicators of the amount of data available in each trial. The maximum number of masts in the cloud at any one time determines how representative our area-averaged concentrations are. It tends to increase with Ri_0, since in lower wind speeds the clouds spread wider while within the instrument array. Values for Phase II are generally larger because additional masts were deployed near the release point. Trials 25 and 27 produced small amounts of data because of poor wind directions.

The lengths of time for which significant non-zero concentrations were measured at one or more masts decrease with wind speed because the cloud is blown away more quickly. Except for Trial 27, the durations for the Phase II trials are consistent with those for flat ground.

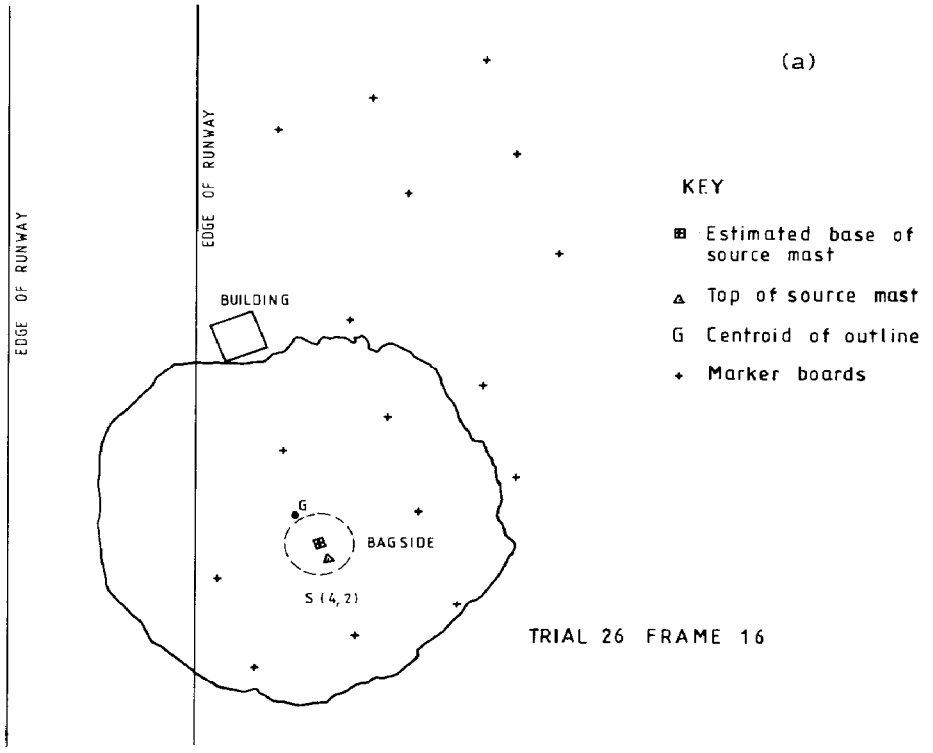

Fig. 1. Cloud outlines traced from overhead photographs in Phase II. (a) Trial 26, 16 seconds after release. (b) Trial 21, 17 seconds after release.

2. Analysis of overhead visual records

Cloud outlines were traced by hand and the area and centroid position in each frame were determined as described in [1] and [3]. There was one difference for the Phase II trials because the base of the source mast could not be see in any trial. However, the introduction of a grid of white marker boards at 25 m intervals on the ground made it possible to infer the position of the spill point in each frame, and in fact gave more self-consistent results than in Phase I for the early centroid movement.

The general quality of the results was very similar to that for Phase I. In particular, the presence of obstacles had little effect on the variation of cloud area with time. Partly this was because the cloud was becoming too faint to see as it reached the obstacles, which were at a radius of 50 m. Figure 1 shows examples of cloud outlines. For Trial 26, Fig. 1(a) shows the cloud front about to engulf the building, and there is a hint of a slight indentation in the front – unfortunately this was the last frame on which the outline was visible. For Trial 21, Fig. 1(b) shows the front within a second or so of hitting the 5 m

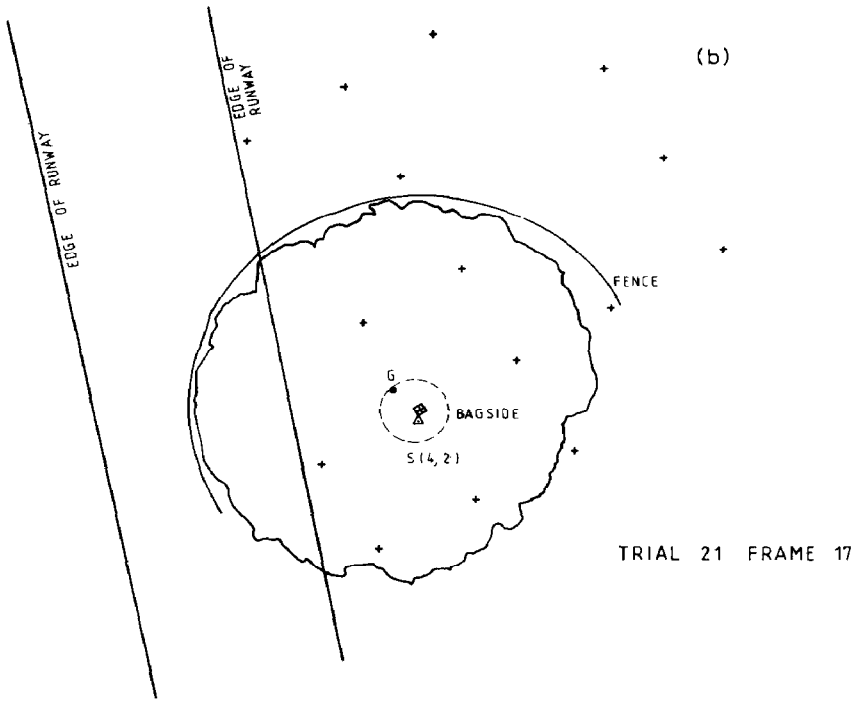

fence. Up to this point, the cloud area had followed the characteristic linear increase with time. Two more frames could be traced and they showed a significant levelling-off of the area graph. These points were ignored in making a straight-line fit.

Table 2 lists all the results of the analysis. The area data are summarised in the Froude number K, which is the area-increase rate normalised by the square-root of the buoyancy as in eqn. (4) of [1]. The values from the building and barrier trials are entirely consistent with the results of Phase I in Table 1 of [1], which led to a recommended value of 1.07 for K (this value is slightly different from that given in [1], which included values for some clouds of which part was invisible against the runway). Thus the initial gravity-spreading behaviour of the clouds is unaffected until the front gets very close to even such a severe obstacle as the 5 m fence.

Since concentration results for Trials 5 and 6 are given in this paper, results from photographic analysis of these are also included in Table 2. The values of the initial volume V_0 and K for Trial 5 have been altered from [1] in the light of the revised estimate of the release volume. Both the cloud speed and the Froude number are anomalously high. This is probably due to an error in recording the timing of the overhead photographs – estimates of the area and centroid position from side-view photographs, on which the time was imprinted,

TABLE 2

Area-increase and cloud-speed results from overhead photographs

Trial no.	Wind speed (m/s)	Cloud speed, U_c (m/s)	Density ratio ρ_0/ρ_A	Initial volume (m^3)	Cloud area increase rate (m^2/s)	Froude no., K
(a) Flat-ground trials						
5[a]	4.6	4.28 (2.86[d])	1.69	1333	500 (244[d])	1.47 (0.89[d])
6	2.6	1.40	1.60	1580	292	0.85[b]
34	1.4	– (0.44[d])	1.83	2100	No overhead photographs (629[d])	(1.35[d])
(b) Building trials						
26	1.9	0.84	2.00	1970	536	1.09
27	2.2	–	4.20	1700	No overhead photographs	
28	9.0	3.27	2.00	1850	500	1.05
29	5.6	–	2.00	1950	No overhead photographs	
(c) Barrier trials (*denotes permeable barrier)						
20	5.7	1.56	1.92	1920	535	1.15
21	3.9	0.86	2.02	2050	594	1.17
22	5.9	0.56	4.20	1400	755	1.02
23*	5.8	1.43	1.92	1850	470	1.07
24*	6.8	1.59	2.03	1925	518	1.05[c]
25	1.4	–	1.95	2000	No overhead photographs	

[a]Container fell in two stages.
[b]Significant portion of cloud not visible against runway.
[c]A small portion of cloud not visible against runway.
[d]Estimates from side-view photographs.

give considerably lower values [12]. The technique of using side-view photographs has also been applied to other Phase I trials, where it is found that cloud centroid speeds can be estimated well but areas are usually somewhat overestimated. In the absence of overhead photographs, this method has also been applied to Trial 34 with results as given in Table 2.

The results for centroid speed show that the fence and the permeable barrier do have a big effect on the translational cloud movement. As in Phase I, the raw data permitted a straight-line fit to determine the speed but the result is generally about a quarter of the upwind 10 m windspeed, instead of about a third to a half on unobstructed flat ground (see Table 4 below and Table 3 of [1]). For Trial 22, the speed was less than 10% of the windspeed, perhaps because of this cloud's high density and large inertia (see Table 1).

Cloud speeds with the building were typical of releases on flat ground.

3. Analysis of arrival and departure times

3.1 Review of method and results for Phase I

The overhead photographs give results only in the early stages of each release, while the cloud remains within 50 m of source. Since the concentration measurement array extends to over 500 m from the source, we developed a method for using the concentration data to track the development of the cloud boundary [1,4]. This involved using the pattern of masts affected by gas to estimate a curve on the ground called the "cloud envelope", defining the area in which gas was present at any time. Arrival and departure times for each mast were gauged from concentration records by eye. Each mast then gave an estimate of the position of the centre of curvature of the upwind or downwind edge of the cloud at those particular times. It was found that the positions deduced from the arrival data gave a fairly consistent linear variation with time. The departure time data were much more difficult to determine and gave rather scattered estimates for the position of the upwind edge. Nevertheless a linear fit for the upwind centre of curvature gave results that seemed reasonably consistent from trial to trial. The estimated cloud areas were generally found to increase somewhat faster than implied by the gravity-spreading law of the early stages. Also the clouds tended to become somewhat elongated, with length-to-width ratios up to two.

Wheatley et al. [6] found that the cloud speed, defined as the means of the speed of the upwind and downwind centres of curvature determined as above, was a good indicator for the turbulence level causing dilution of the cloud. It allowed a better correlation of the concentration data by a simple box model than either the 10 m windspeed or the vertical rms turbulent velocity. This comes about because the cloud speed as a fraction of windspead decreases quite strongly as a function of initial Richardson number (see Fig. 5 of [6]).

In this paper, results are reported for the three flat-ground trials not analysed in [1], and for the building trials, where the building was expected to have very little effect on the outer cloud boundary (except in its immediate neighbourhood). Also it was found that the method gave reasonable results in Trials 20–24, where the barriers might have been expected to cause quite complex cloud development.

3.2 Examples of results

The Trials chosen are those already illustrated by Fig. 1, i.e. Trials 26 and 21.

Trial 26 (building)

The first part of the analysis is the determination of a range of possible cloud envelopes. Figure 2(a) is a plan of the sensor array showing where gas was detected during Trial 26. The wind direction was very close to the axis of the

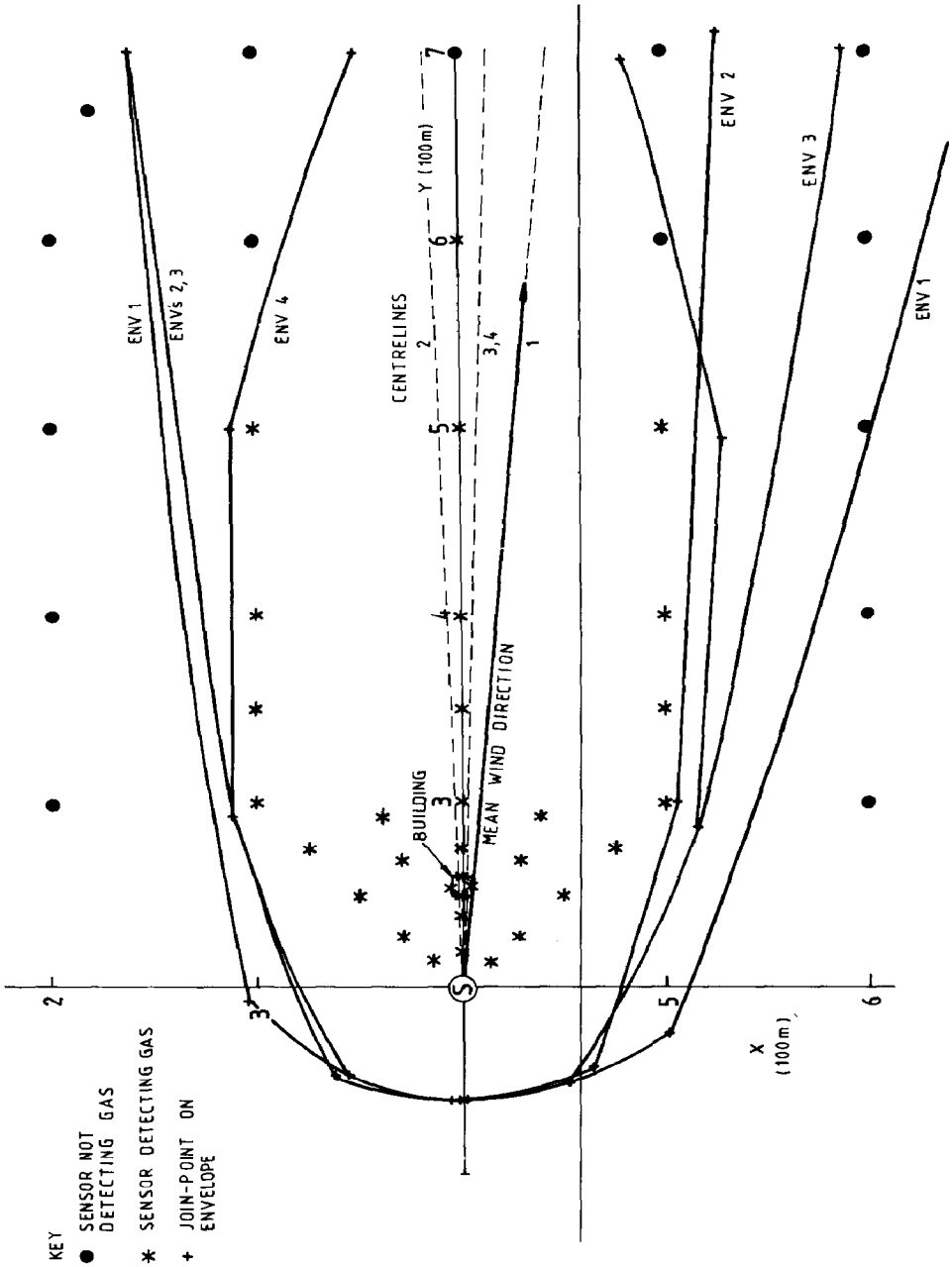

Fig. 2(a). Cloud envelopes for Trial 26.

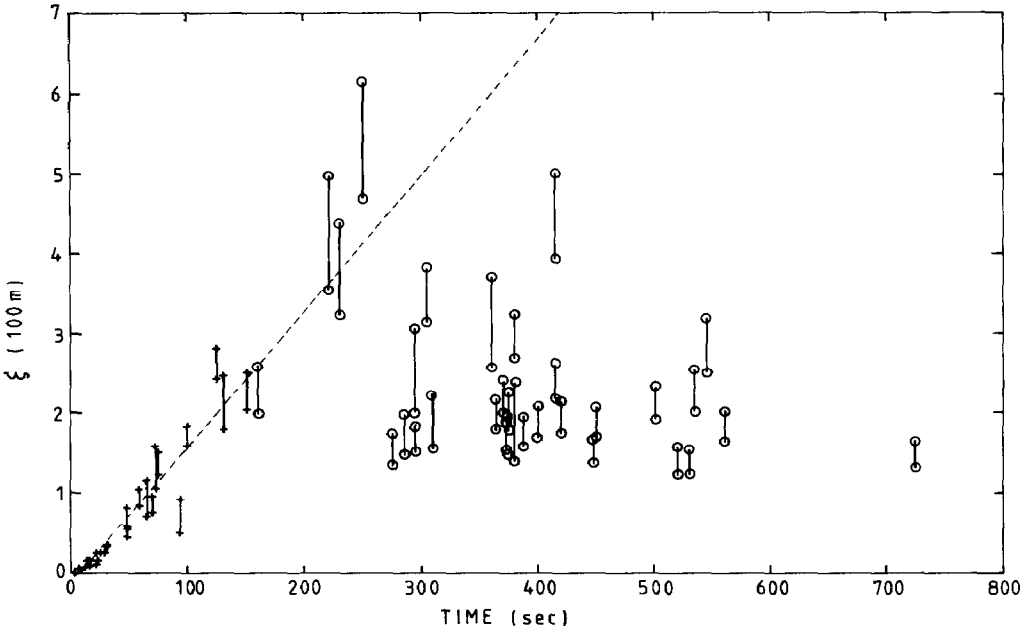

Fig. 2(b). Apparent cloud-centre displacements, Trial 26: +, based on arrival times, ⊙, based on departure times. Vertical lines indicate range due to alternative cloud envelopes. — — —Best-fit straight line for envelope 3.

array so both sides of the envelope fell within the array. This trial is unique in Phases I and II in having a ground-level sensor which detected no gas only 500 m from the source on the path of the cloud centroid (at $(X, Y) = (4,7)$). Thus the rate of dilution of the cloud with distance must be one of the most rapid recorded in the trials. The initial Richardson number was similar to those of Trials 8 and 17 but the Pasquill stability category was B instead of D or E. This atmospheric instability seems more likely to account for the rapid dilution than the influence of the building wake, which, as seen from Fig. 2(a), would have affected a much narrower area than the cloud envelope.

Four cloud envelopes were tried. No. 1 was based on the actual wind direction and was designed to pass outside (3,3), but was found to expand too far on the right-hand side. It was also intended to represent the real cloud envelope, and so continued to widen downwind, rather than contract to represent the apparent envelope limited by the sensitivity of the instruments. Envelopes 2 and 3 were obtained by swinging the cloud path to the left to varying extents and making slightly different assumptions near the source. Envelope 4 was an estimate of the apparent cloud envelope, or equivalently the contour of maximum concentration of around 0.05% (see [1]).

Envelope 3 was regarded as the mosts realistic option because it gave a some-

what better result for the mass balance than Envelope 2 and avoided engulfing any of the non-responding sensors along $X=2$ and $X=6$.

Figure 2(b) shows the results of calculating $\xi_{\pm}$ from eqn. (11) of [1] for each of the masts detecting gas and plotting the results for ξ_- against the corresponding arrival times and for ξ_+ against the departure times. In each case the range produced by using all the envelopes of Fig. 2(a) is indicated. As found in the Phase I trials the results are reasonably consistent for the downwind edge of the cloud. Though the wide range of possible envelopes gives considerable uncertainty, the straight-line fit based on the results with Envelope 3 looks a good representation of the overall speed of the cloud's downwind part.

With the departure time data, the situation is similar to that of the high-Ri_0 trials in Phase I, with a large scatter of departure times with no significant correlation with a moving upwind edge of the cloud. It appears that the upwind portion of the cloud was fairly stationary and that signals ceased because of dilution of the cloud, not because it moved away downwind. It was judged appropriate to represent the position of the centre of curvature of the upwind edge by the constant value $\xi_+ = 200$ m.

Trial 21 (5 m fence)

There was some doubt about whether it was appropriate to apply the idea of a smoothly expanding cloud outline to releases perturbed by a major obstacle such as the fence or screen. However in all cases, the pattern of masts on the ground did allow the fitting of envelopes as readily as in the Phase I trials. Trial 25 was not analysed because the wind blew most of the cloud away from the sensor array, and no overhead photographs were taken to provide an alternative estimate.

In Trial 21, Fig. 3(a) shows that the right-hand side of the envelope was tightly constrained by the responding sensors at (4.5, 2.5) and (5,6) and by those not detecting gas at (4.75, 2.75) and (5,5). Using the mean wind direction then gives a left-hand side which goes beyond the non-responding sensor at (2.2, 6.7). Taking cloud paths more to the right remedies this but it becomes somewhat difficult to get the point (3,3) inside the envelope in a convincing fashion.

This selection of envelopes then generates the plot of cloud-centre displacements shown in Fig. 3(b). The self-consistency of the arrival times is quite good, and comparable to that in many Phase I trials. The influence of the fence may perhaps be discerned at points with $\xi_- < 50$ m, which are rather more erratic than for flat-ground trials. However the straight line fitted to the data for Envelope 3 as a reasonable compromise seems a good indicator of behaviour at larger distances well downwind of the barrier.

The departure results show a more discernible trend than in Trial 26 except for the points upwind of the barrier. These show an anomalously long persist-

ence of gas up to the end of the data-recording period at 600 s. This is because a certain part of the cloud remains in the rather stagnant region upwind of the barrier. The points have been excluded from the regression analysis to find the movement of the rear edge of the cloud in Fig. 3(b). This persistence is also very noticeable in a direct comparison of individual sensor records with those from corresponding positions in Trial 7, which had a similar windspeed and Richardson number [13, section 21.2.4].

3.3 Summary of results and calculation of cloud areas

The results of the cloud envelope analysis for the Phase II trials and the three flat-ground trials not covered by [1] are summarised in Tables 3 and 4. Table 3 gives the parameters ξ_i and R_i^2 needed to generate the selected cloud envelope for each trial from eqns. (8) and (12) of [1]. Table 4 gives the equations of the straight lines fitted to the results of calculating $\xi_\pm$ for all the relevant sensor masts and plotting them against the arrival and departure times. For this regression analysis, departure times for points upwind of the barrier in Trials 20–24 were generally omitted for the reasons given in the description of the Trial 21 above.

Table 4 also lists the speeds of the apparent centre of the downwind cloud edge $\dot{\xi}_- = d\xi_-/dt$ as a fraction of the mean windspeed at 10 m, $\bar{U}_{10}$. A plot of these values against the initial Richardson number Ri_0 from Table 1 shows a decreasing trend indistinguishable from the results for Trials 7–19 listed in Table 3 of [1] (see also Fig. 5 of [6]). One point is rather erratic, that for Trial 26 with the highest value of $\dot{\xi}_-/\bar{U}_{10}$ of any trial – we have already seen above that it is rather difficult to establish a satisfactory cloud envelope in this case.

Thus over these distances up to 45–90 fence heights downwind, the local reduction of windspeed near the fences (illustrated in Fig. 11 of [14]) seems completely insignificant in the translational motion of the leading part of the clouds. However, it may be that reductions in cloud velocity at a fixed height are counterbalanced by increases in cloud height downwind of the barriers (see below).

Interpretation of the results in Table 4 for the trailing edge of the cloud in the barrier trials is complicated by the retention of gas upwind, which has been ignored in the analysis. The rear edge in Trials 23 and 24 with the permeable barrier moves much more slowly than in the comparable flat-ground trials, 13 and 16 (see Table 3 of [1]). This is corroborated by comparisons of individual sensor records downwind of the barrier in Fig. 21.2 of [13] and in [15]. In the trials with the impermeable barrier, there must have been concentrations of gas below the detectable level in the region between the obstacle and the estimated rear edge of the cloud, as gas was slowly dispersed from the portion of the cloud trapped upwind of the barrier. It is merely a coincidence that the

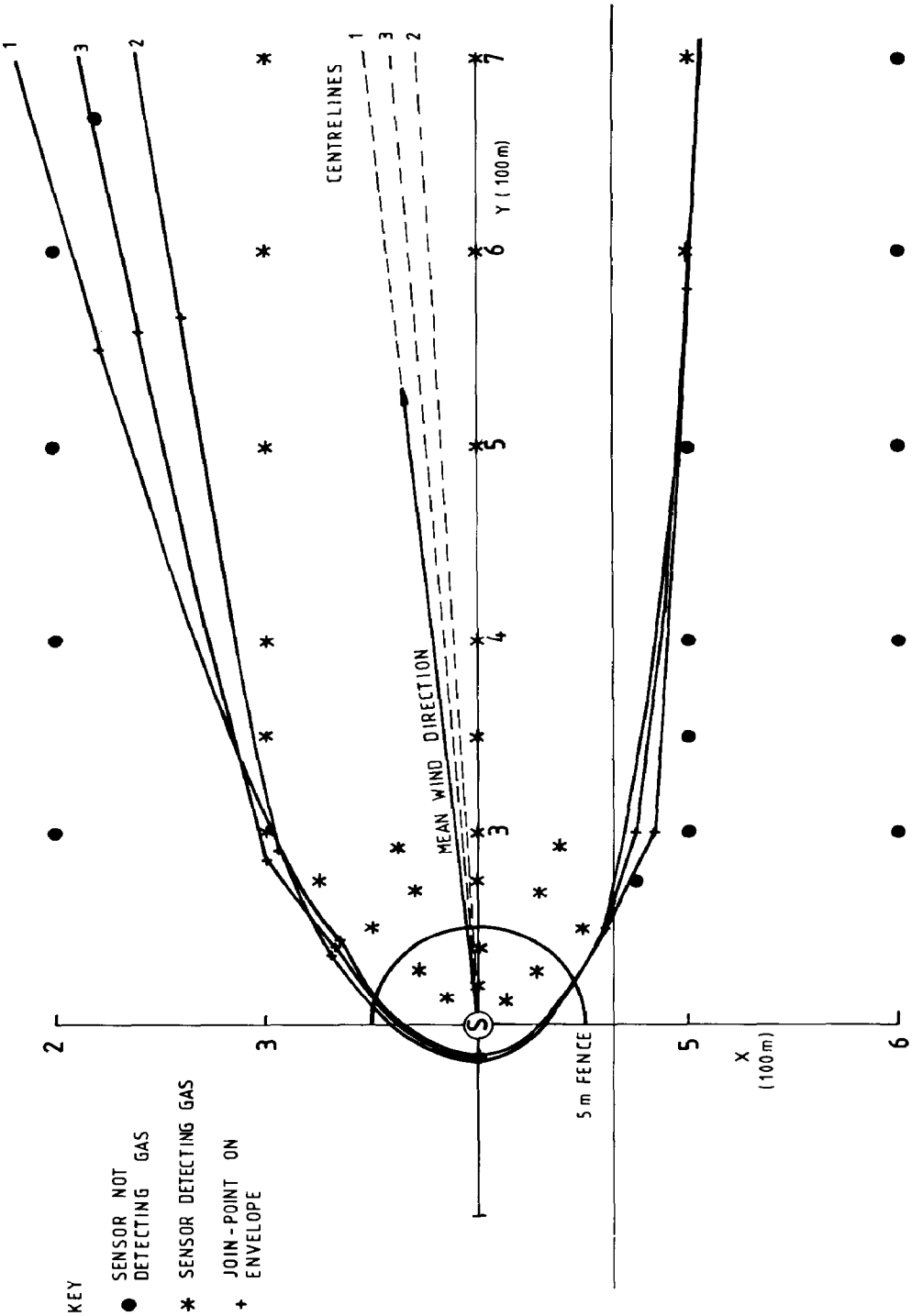

Fig. 3(a). Cloud envelopes for Trial 21.

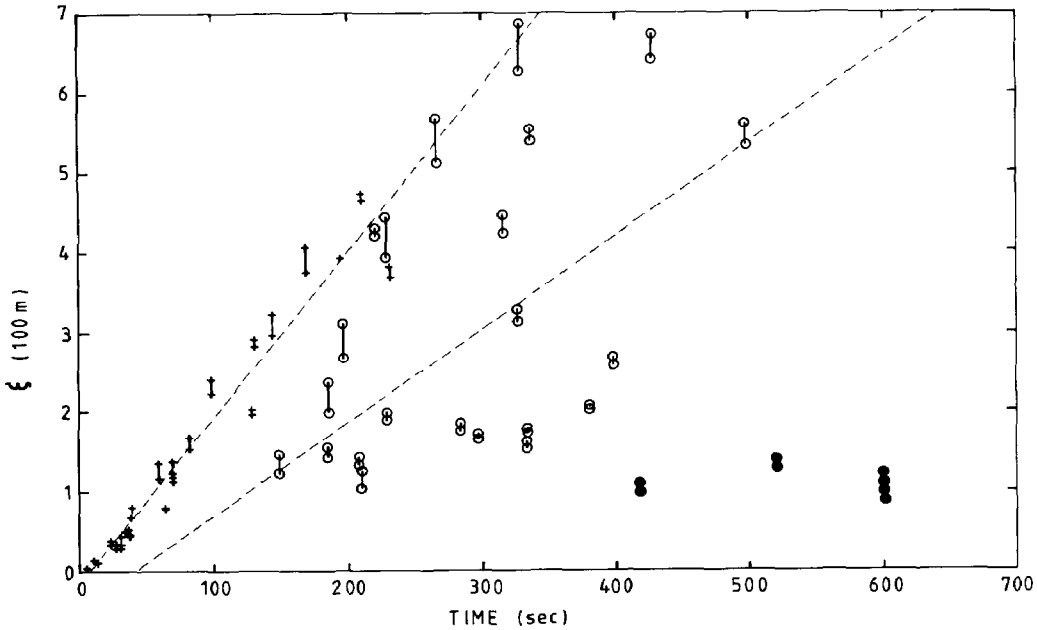

Fig. 3(b). Apparent cloud-centre displacements, Trial 21: +, based on arrival times; ⊙, based on departure times, downwind of the barrier; ●, based on departure times, upwind of the barrier. Vertical lines indicate range due to alternative cloud envelopes. — — —Best-fit straight lines for envelope 3.

apparent rear edge of the cloud moved at a speed typical of the flat-ground trials.

Cloud areas

Figure 4 gives the results of using the correlations of Table 4 for cloud geometry to calculate cloud areas, by assuming an instantaneous outline consisting of two circles joined by their common tangents [1,4]. The plots follow exactly the same format as Fig. 8 of [1] with the area being shown as a proportion of the value extrapolated from the gravity-spreading law established from the visual analysis. The abscissa is the dimensionless time τ given by eqn. (3). The correlations are not expected to be accurate enough near the origin, as they are fitted to cloud movement through the whole sensor array (cf. Figs. 2(b) and 3(b)), so for $\tau < 50$, the area A is taken as $A_0\tau$ where A_0 is the initial area, and for $50 \leqq \tau \leqq 100$, as a linear combination of this value and that obtained from the regression analysis using eqn. (16) of [1].

The results for the three flat-ground trials in Fig. 4(a) run somewhat counter to the trend found previously in Phase I. Trial 5 was at a low Richardson number but displayed a much slower area increase rate than trials at similar Ri in Phase I – also little cloud elongation was found. Trial 6 also gave rather low

TABLE 3

Parameters defining cloud envelopes

Trial no.	Centreline direction θ^c (decrees)	Values of distance from source, ξ^a, and square of cloud radius, R^b, used to generate envelope							
		ξ_1	R_1^2	ξ_2	R_2^2	ξ_3	R_3^2	ξ_4	R_4^2
(a) Flat-ground trials									
5	3.21	0.627	0.315	3.334	0.667	5.055	0.670	–	–
6	−33.69	0.798	0.532	1.371	0.725	5.283	0.938	–	–
34	56.31	1.215	4.786	1.948	5.543	3.545	4.641	–	–
(b) Building trials									
26	1.91	0.300	0.724	1.158	1.202	5.158	2.064	–	–
27	−132.70	0.598	2.022	1.376	3.511	–	–	–	–
28	−41.88	0.155	0.073	0.820	0.377	2.155	0.569	–	–
29	−27.00	0.345	0.222	1.838	0.717	4.289	2.177	–	–
(c) Barrier trials (* denotes permeable barrier)									
20	0	0.748	0.373	5.051	0.813	–	–	–	–
21	4.64	0.841	0.557	1.233	0.913	3.861	1.724	–	–
22	2.29	0.958	0.558	2.101	0.759	5.084	1.000	–	–
23*	−39.09	0.300	0.189	0.654	0.517	1.038	0.622	5.771	0.634
24*	−38.29	0.300	0.238	0.603	0.502	4.412	0.777	–	–
25	[d]								

[a]Unit 100 m.
[b]Unit 10^4 m^2.
[c]Note that the sign convention for θ is opposite to that used in the HSE hardcopies of data for wind heading.
[d]Poor wind direction: analysis not carried out.

areas but they were comparable to those in Trial 17, which gave the lowest values in Phase I [1]. Trial 34 did give a similar pattern to Trials 9 and 12 at high Richardson numbers, though there is additional uncertainty in these cases as only one edge of the cloud envelope was captured within the instrument array.

With the building present, Fig. 4(b), there was no significant difference in the overall pattern of the results but Trial 28 gave rather small results for such a low Richardson number. In the case of the barrier trials, Fig. 4(c), there is a distinct tendency for the estimated areas to remain around 3/4 of the gravity-spreading value. This seems quite natural as part of the cloud is trapped by the semicircular fence and so is not free to slump. As mentioned above, we have ignored the departure times for gas upwind of the fence in determining the

TABLE 4

Correlations for distances from source of apparent centres of downwind and upwind edges of cloud

Trial no.	Apparent centre based on arrival times, ξ_- (units 100 m and 100 s)	Apparent centre based on departure times, ξ_+ (units 100 m and 100 s)	$\dot{\xi}_-/\bar{U}_{10}$	$U_c/\bar{U}_{10}$ (from Table 2)
(a) Flat-ground trials				
5	$3.24t-0.50$	$2.36t-0.21$	0.70	(0.62)[c]
6	$2.21t-0.41$	$0.73t+1.06$	0.85	(0.54)
34	$0.65t-0.04$	$0.18t+1.85$	0.46	(0.31)[bc]
(b) Building trials				
26	$1.70t-0.14$	$+2.00$	0.89	(0.44)
27	$1.10t-0.01$	$0.05t+1.53$	0.50	[b]
28	$5.64t-0.35$	$5.64t-0.85$	0.63	(0.36)
29	$3.46t-0.18$	$2.91t-1.15$	0.62	[b]
(c) Barrier trials (* denotes permeable barrier)				
20	$3.30t-0.30$	$2.11t-0.81$	0.58	(0.27)
21	$2.07t-0.16$	$1.17t-0.48$	0.53	(0.22)
22	$2.61t-0.17$	$1.63t-1.37$	0.44	(0.09)
23*	$3.76t-0.36$	$0.84t+0.40$	0.65	(0.25)
24*	$2.86t-0.30$	$0.31t+1.20$	0.42	(0.23)
25	[a]			[b]

[a]Poor wind direction: analysis not carried out.
[b]Overhead photographs not available.
[c]Estimated from side-view photographs.

motion of the upwind edge of the cloud, so our results in Fig. 4(c) refer to the downwind portion of the cloud, which has a reduced buoyancy content.

4. Area-averaged concentrations

4.1 Modifications needed to the procedure

The method of averaging the concentration records over the horizontal extent was adopted in [2] for the Phase I trials for two main reasons. First, the area-averaged ground-level concentration is close to the volume-average which is predicted by the simple box-models of dispersion. Second, it makes use of all the data available and should even out the effects of fluctuations at individual sensors. In both these respects, it seems preferable to the frequently adopted method of comparing box-model predictions with the maxima at individual sensors as functions of position. The disadvantages are that much more data processing is needed to produce area averages and that it is not always easy to

determine gas departure times which define the position of the upwind edge of the cloud [16].

The results for Phase I [2] were very satisfactory. With the exception of one or two trials, with small numbers of masts in the cloud, the individual results were very self-consistent in giving a smooth decrease of concentration with time. When plotted together in dimensionless form, the graphs displayed

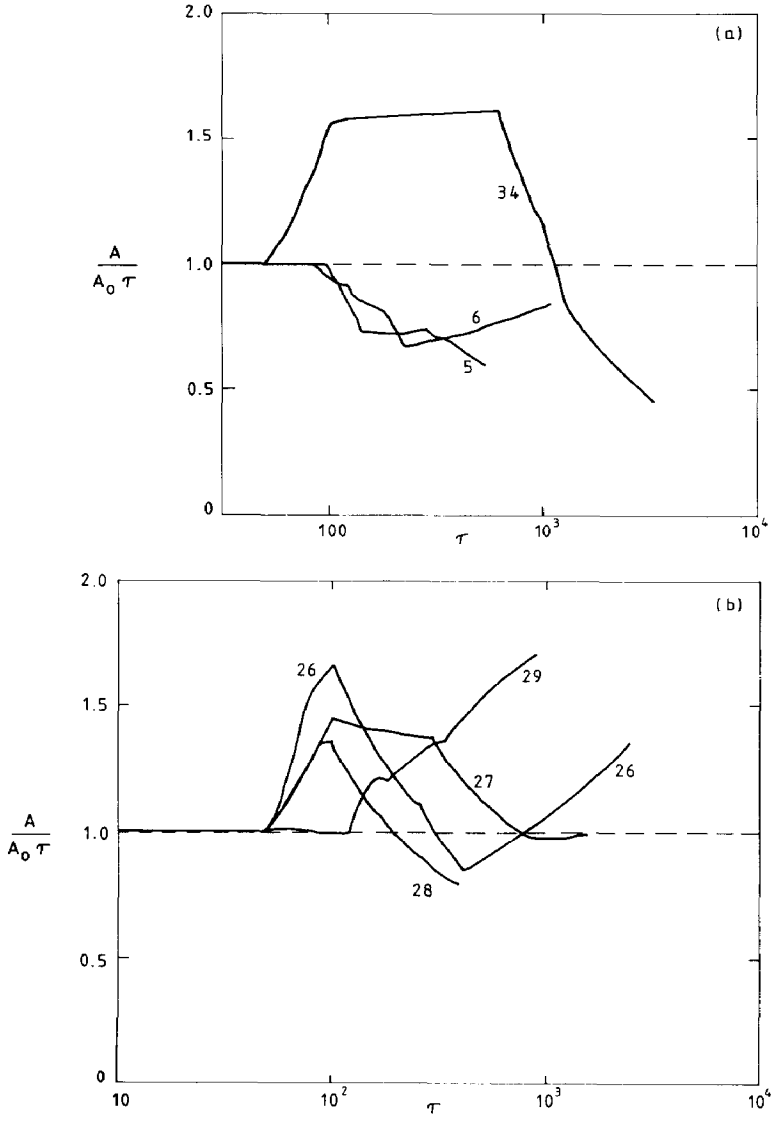

Fig. 4. Ratio of cloud area as determined by cloud envelope analysis to area expected from gravity-spreading law. Trial numbers are indicated on graphs. (a) Flat-ground trials. (b) Building trials.

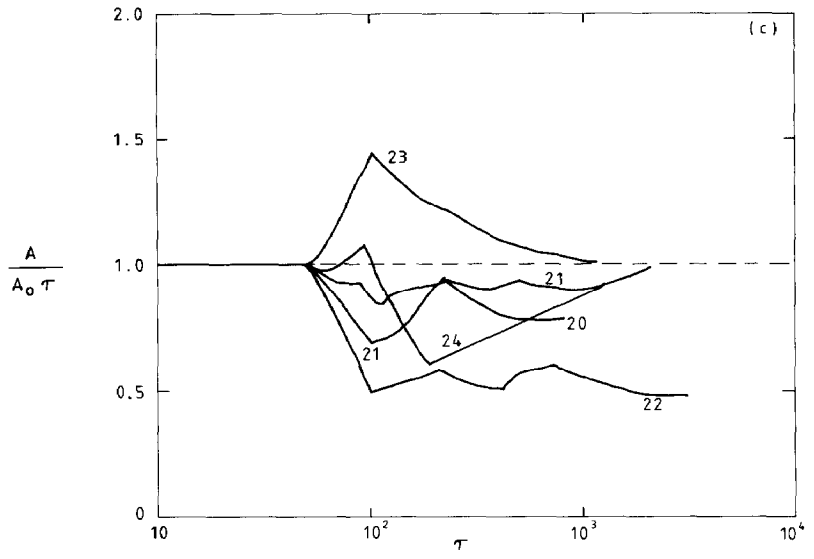

Fig. 4 (continued). (c) Barrier trials.

features corroborating the main principles of simple box-models. At small times the data collapsed with a small dilution rate characteristic of edge entrainment. At larger times, the concentration started to decrease more rapidly because of top entrainment. The results in this regime were ordered according to the initial Richardson number. Wheatley et al. [5,6] established a set of entrainment coefficients which gave a very good fit across the whole range of Trials 7–19, by using the cloud speed as the velocity scale for top entrainment, rather than the wind speed or external turbulent velocity.

In this paper the area-averaging analysis is applied to the three flat-ground trials not included in [2]. The Phase II trials are also analysed. In the case of the building, it was expected that the results could be regarded as further data for testing Wheatley et al.'s correlation, since the building occupied a very small region compared to the area of the cloud (cf. Fig. 2(a)). For the barrier, it was decided to calculate area averages for the upwind and downwind portions of the cloud *separately*, so as to display the diluting effect of the obstruction on the cloud as a whole. The effect of the barrier has also been assessed by comparison with overall results for Phase I trials at comparable Richardson numbers.

In Phase II, the array of masts was considerably altered, mainly to improve spatial resolution near the source [13]. This necessitated one change in the procedure described in [1]. Since in Phase I, the masts were roughly uniformly spaced, the concentration measurements at each time were summed with uniform weighting. In Phase II, each measurement was weighted according to the proximity of the mast to its neighbours. The weighting was simply the area of

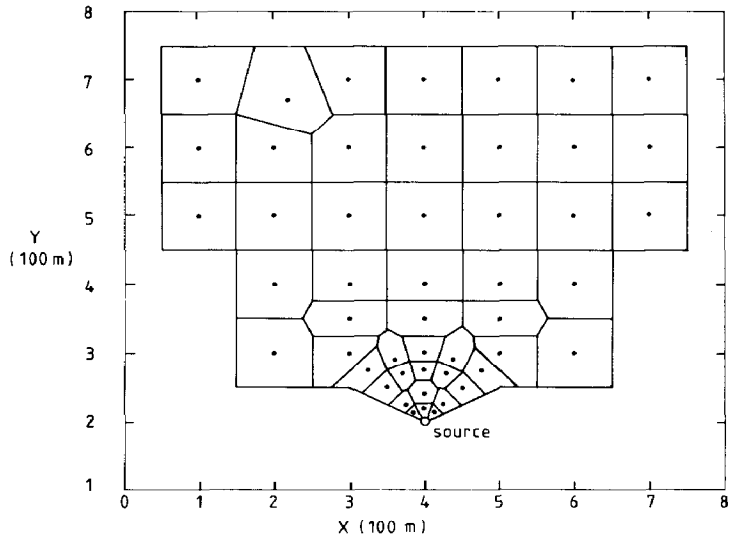

Fig. 5. The standard array of gas sensor masts in Phase II and the polygons defining the weighting for each in the horizontal averages. There were variations in several trials, e.g. beause of extra sensors attached to the building.

the set of points on the ground nearer to the mast in question than to any other. The experimental region is thus divided into the polygonal zones shown in Fig. 5. An outer boundary to the region covered by the sensors also had to be defined – it was taken at a distance equal to half the typical spacing of sensors in the locality.

For numerical evaluation, we did not attempt to calculate the areas of the polygons exactly. Instead, the area covered by masts was divided up into small squares of side 4 m near the source (for $3<X<5$ and $Y<3$) and side 20 m further away. The area of each square was added to the weighting of the mast nearest its centre.

In this way, the area-averaging produces results which are not biased towards any particular part of the cloud.

4.2 Flat-ground trials

Figure 6 shows ground-level area-averaged concentrations for the flat-ground Trials 5, 6 and 34. The data are plotted in the same dimensionless form as used for Trials 7–19 in [2] with τ defined by eqns. (1)–(3). Also included in Fig. 6 are the predictions from the correlation of Wheatley et al. [5,6] based on cloud speed, i.e. with

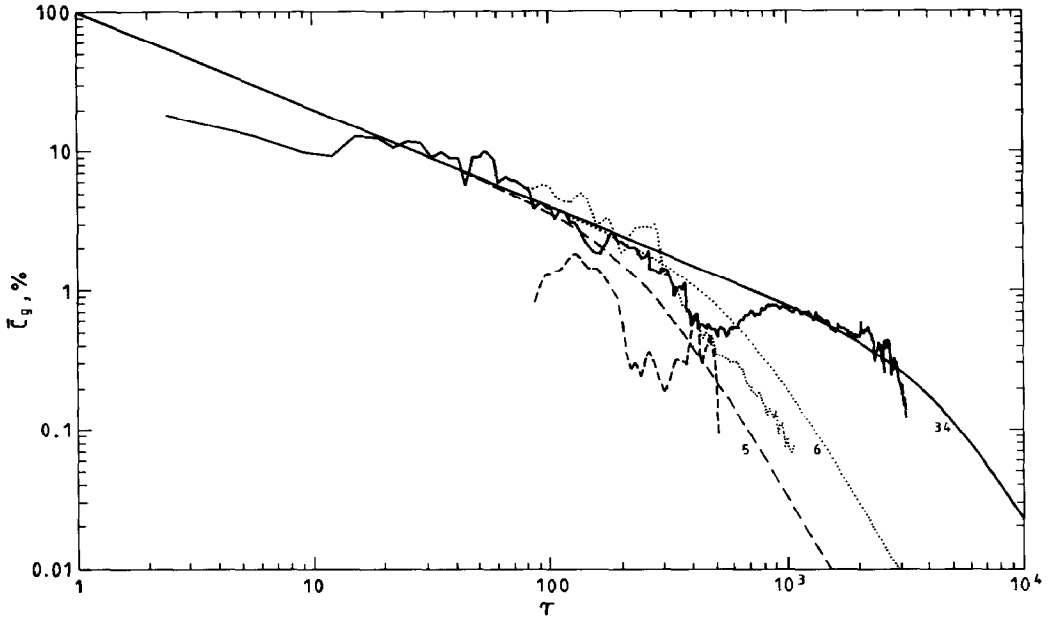

Fig. 6. Flat-ground trials: mean ground-level concentrations versus dimensionless time, τ; also predictions from a correlation of Wheatley et al [5]. Trial numbers shown against graphs.

$$\alpha_E = 0.7,\ \mu = 1,\ \alpha_T = 0.14 \text{ and } U = 0.16\ U_c \qquad (4)$$

in the generalised Picknett model, where α_E is the edge entrainment coefficient, μ the power of the Richardson number in the top-entrainment relation, α_T the top-entrainment coefficient and U the velocity scale. U_c is the cloud speed, defined as the arithmetic mean of the speeds of the front and rear centres of curvature of the cloud edges as listed in Table 4.

The results for the low-windspeed case, Trial 34 follow the prediction well. The data extends to much earlier times than for the Phase I trials because of the revised instrument lay-out. The edge-entrainment behaviour is well shown except for the first few points when gas is only just entering the sensor array. The curious dip in the data around $\tau = 500$ does not seem to have any particular cause and probably reflects just a temporary bias in concentrations in the part of the cloud being sampled at the time – the path of the cloud was well off the axis of the sensor array.

For Trial 6, the match between prediction and data is slightly worse than in most of the trials analysed previously (see Figs. 22–34 of [5]) but not significantly so. In Trial 5, the cloud envelope was very narrow because of the small volume eventually released and passing down the array axis it affected only one row of sensors, so that only a small number of measurements contribute to the averages. This accounts for the erratic nature of the data, but the low concentrations recorded compared with the prediction may represent a significant effect of atmospheric stability (see also Trial 26 below). This trial was

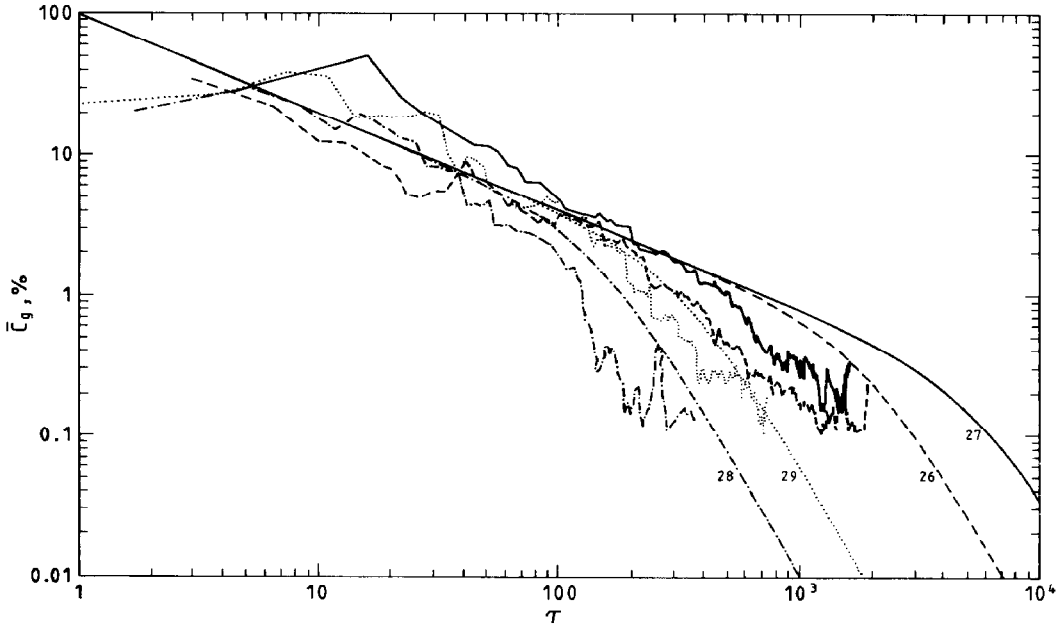

Fig. 7. Phase II building trials: mean ground-level concentrations versus dimensionless time τ; also predictions from a correlation of Wheatley et al. [5]. Trial numbers shown against graphs.

thought to be the only one in Phase I with definitely unstable conditions, assessed as Pasquill category B [17]. Davies and Singh ([18], Fig. 20) did not find particularly high atmospheric turbulence intensities for this trial. On the other hand, after a more extensive analysis of the meteorological data, Puttock [19] assigned the category B or B/C to Trials 8 and 15 as well as Trial 5.

4.3 Building trials

Figure 7 shows the horizontally averaged ground-level concentrations for all four trials with a cubical building, and also the predictions from Wheatley et al.'s [5,6] correlation using parameter values (4). The results were rather a surprise. The curves all show the common early edge-entrainment phase, albeit with considerable scatter, but in all cases the downturn into the top-entrainment phase begins too early. The discrepancy is most serious in Trial 26 with concentrations about $3\frac{1}{2}$ times less than the correlation for τ around 1000. The divergences are also significant in Trials 27 and 28, while in Trial 29 the match is comparable to some of the Phase I trials.

The extent of these divergences is quantified in Table 5 which corresponds to Table 11 of [5]. This shows the results of optimising the value of α_T in eqn. (4) while keeping the parameters α_E and μ fixed. The goodness of fit between data and model was gauged by the GFMs (goodness-of-fit measures) S_2 and

TABLE 5

Values of $\alpha_T{}^o$ and $\alpha_T{}^\pm$ for GFMs S_2 and S_5 and the model $U=0.16U_c$, $\alpha_E=0.7$ and $\mu=1$. The range of α_T examined was $0.001 \leqq \alpha_T \leqq 5$

Trial no	S_2			S_5		
	$\alpha_T{}^-$	$\alpha_T{}^o$	$\alpha_T{}^+$	$\alpha_T{}^-$	$\alpha_T{}^o$	$\alpha_T{}^+$
(a) Flat-ground trials						
5	0.35	0.78	>5[a]	0.16	0.33	0.50
6	0.24	0.28	0.33	0.18	0.24	0.34
34	0.042	0.37	2.79	0.049	0.28	0.52
(b) Building trials						
26	1.39	3.00	>5[a]	0.47	1.00	1.56
27	–	>5[b]	–	–	>5[b]	–
28	0.53	0.78	1.38	0.14	0.35	0.52
29	0.16	0.28	0.56	0.12	0.20	0.27

[a]S_2 less than twice minimum at $\alpha_T=5$.
[b]Minimum of GFMs beyond end of range of α_T examined.

S_5. S_2 and S_5 embody different intuitive methods of allowing for the differences in significance of the calculated mean concentrations, which arise because of the varying sample size. As well as the optimum value $\alpha_T{}^o$ needed to minimise the GFMs, Table 5 also shows the interval $(\alpha_T{}^-, \alpha_T{}^+)$ for which the GFM is less than twice its minimum. This is a measure of the uncertainty in fixing $\alpha_T{}^o$ for a particular trial. For reasons discussed in [5], it is not relevant to compare values of the GFMs for different trials.

For Trials 7 to 19, it was found in [5] that the best overall value of α_T was 0.14, though this did not fall within the interval $(\alpha_T{}^-, \alpha_T{}^+)$ in every case. This gave the excellent visual fit of data and correlation seen in Figs. 22–34 of [5]. By comparing Table 5 with Table 11 of [5], it will be seen that the range $(\alpha_T{}^-, \alpha_T{}^+)$ for Trials 6, 34 and 29 fell within the variability seen in Trials 7–19, and that Trials 5 and 28 are erratic according to S_2 but consistent according to S_5. Trials 26 and 27 remain anomalous with apparent top-entrainment rates an order of magnitude greater than was found in [5]. (Note that the entrainment rate is proportional to the cube of the velocity scale.)

It is tempting to conclude that despite its diminutive size, the building generated enough turbulence to affect overall entrainment into the cloud. However, various other possible contributing factors can be identified. One is that the optimal value of α_T is rather sensitive to errors in estimating U_c at low windspeeds [5], and we have noted above the difficulties in determining the cloud envelope for Trial 26. Also, Trial 26 was the only one in Phase II with a strongly unstable atmosphere, with Pasquill category B, a characteristic shared

with Trial 5. Davies and Singh ([14] Appendix I) report very high turbulence intensities for Trial 26. In Trial 27, the cloud path was away from the sensor array and data was obtained only from the large upwind spread at high Richardson number: thus the data comes from a small, and quite possibly unrepresentative, part of the cloud.

4.4 Concentrations near the building

While it is questionable whether the building affects overall cloud behaviour, McQuaid and Roebuck [13] have shown that there are very distinctive concentration distributions in its immediate neighbourhood. They gave examples for Trial 26. Concentrations at groundlevel in the wake of the building 15 m from its downwind face had much lower peak values and somewhat lower subsequent values than at sensors 30 m to each side (Fig. 21.3 of [13]). The ground-level sensor on the upwind face experienced a very much briefer signal than one 10 m upwind (Figs. 21.14 and 21.15 of [13]). It is also of interest to compare these concentrations with our area-averaged concentrations. This will show how concentrations around a building might compare to expectations

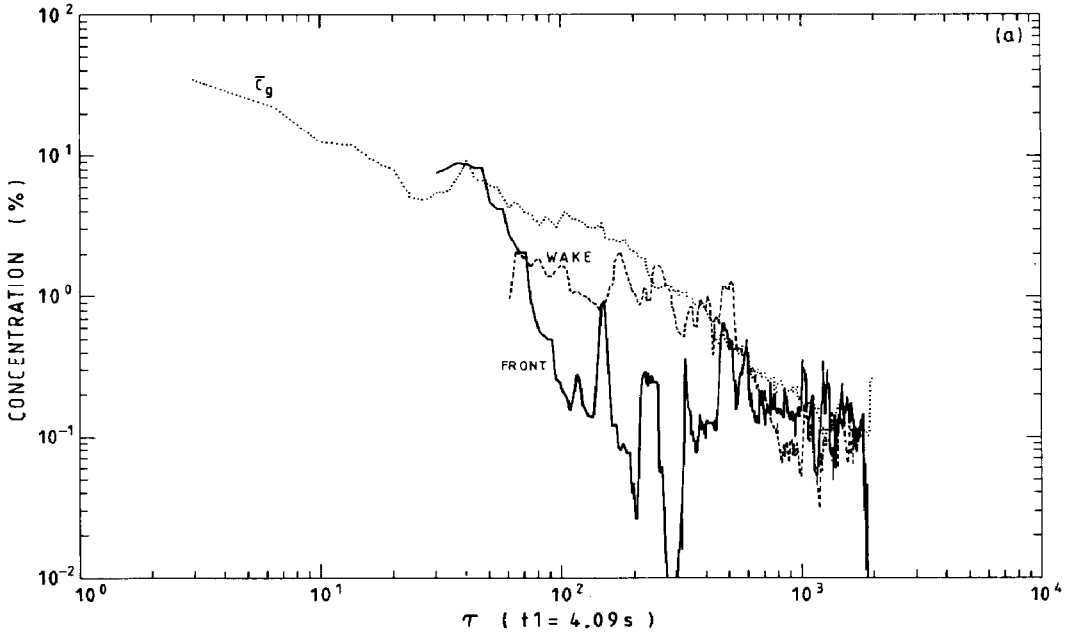

Fig. 8. Phase II building trials: comparison of ground-level concentrations near building with mean cloud values $\bar{C}_g$ as functions of dimensionless time τ (see Section 1.2 for definitions of τ and t_1). (a) Trial 26, $Ri_0 = 1672$ - building on cloud path, concentration on upwind face and mean near-wake concentration. (b) Trial 28, $Ri_0 = 334$ - same positions (c) Trial 27, $Ri_0 = 8233$ - inset diagram indicates position of building and sensors relative to wind direction and gas source.

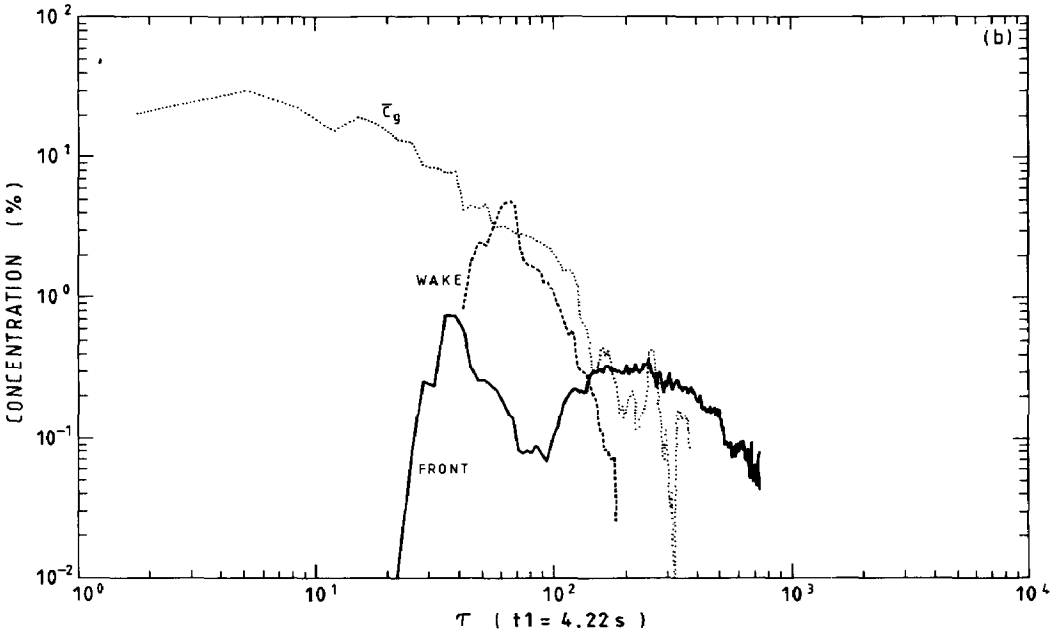
(b)
$\bar{c}_g$
WAKE
FRONT
CONCENTRATION (%)
10^2
10^1
10^0
10^{-1}
10^{-2}
10^0
10^1
10^2
10^3
10^4
τ (t1 = 4.22 s)

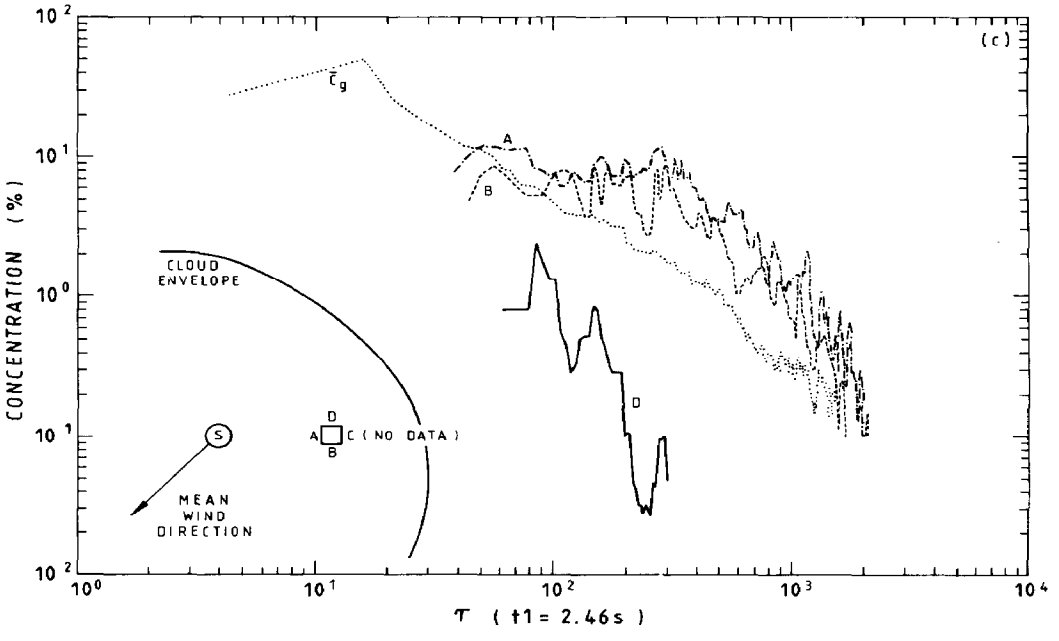
(c)
$\bar{c}_g$
A
B
D
CLOUD ENVELOPE
S
MEAN WIND DIRECTION
D
A C (NO DATA)
B
CONCENTRATION (%)
10^2
10^1
10^0
10^1
10^2
10^0
10^1
10^2
10^3
10^4
τ (t1 = 2.46 s)

based on box-models – this is relevant to assessing hazards to people inside buildings from passing vapour clouds.

Some results are given in Fig. 8. In Trials 26 and 28, traces from the sensor at groundlevel on the upwind face of the buildings are labelled "front": the "wake" values are the average of the corresponding sensor on the rear face and one 15 m downwind, and so are representative of the near-wake region of recirculatory flow. In both cases the concentration at the front has a high initial peak and then becomes very much lower than the cloud average. What is not easily seen in the linear plots of [13] is that subsequently concentrations here increase again and become similar to the cloud average. In Trial 28 it appears that there was a persistent pocket of gas at the upwind face. This late signal was excluded from the calculation of the average as consideration of other departure times showed that the main body of the cloud had drifted well downwind. The effects in the wake are not particularly striking – departures from the overall mean are the expected decreases, but not particularly significant in view of the variability of individual sensor records.

In Trial 27 a late change in wind speed placed the building in quite a different position relative to the source (Fig. 8(c)). It was in the upwind spreading region, which was quite extensive because of the high initial Richardson number. Also its sides were almost exactly at 45° to the oncoming wind, which makes the local wind-field quite different from the case of normal orientation. The gas sensors on the two downwind faces gave very similar results which were somewhat higher than the overall average for the cloud. Only one of the sensors on the upwind faces was functioning: it gave very much lower concentrations, by an order of magnitude or more.

In Trial 29, the building was placed 20 m upwind of the source and was not instrumented. Good photographic data is not available for this trial but Davies and Singh [14] made a wind-tunnel simulation in which they found that gas reached the rear face of the building but did not spread around its sides (see their Fig. 24). We have already seen from Fig. 7 that in this trial there appeared to be little effect of the building wake turbulence on average concentrations in the cloud.

4.5 Barrier trials – mean concentrations and cloud heights Low-Richardson-number cases

To study overall cloud behaviour, we have averaged concentrations separately for the portions of the cloud upwind and downwind of the barrier. In Fig. 9, these are plotted against dimensionless time together with mean concentrations from Phase I trials at similar initial Richardson numbers.

Trials 20, 23 and 24 had initial Richardson numbers Ri_0 of 500, 535, and 574 (Table 1) and can all be compared with Trials 13 ($Ri_0 = 559$) and 16 ($Ri_0 = 572$). In Trial 20 the obstacle was the 5 m impermeable fence; in Trial 23, there were two 10 m permeable screens; and in Trial 24, four screens.

In Fig. 9(a) it is seen that upwind concentrations in Trial 20 remain somewhat high up to $\tau = 200$, and that downwind concentrations are an order of magnitude lower, but after this time the concentrations converge towards the results from flat-ground. The permeable screens appear to have virtually no effect on concentration levels (Figs. 9(b) and 9(c)). However, it should be remembered that the rear of these clouds does move significantly more slowly – although concentrations are similar, these clouds are more elongated than their flat-ground counterparts. The downwind concentration becomes higher than that upwind after $\tau = 250$, probably simply because the region of maximum concentration has moved far enough downwind to bias the two averages over different regions of the cloud.

Rottman et al. [9] predicted several distinctive effects of obstacles on cloud heights, on the basis of simple analysis and idealised laboratory experiments. So we decided to evaluate the height-scale of the vertical distributions of horizontally averaged concentration upwind and downwind of the obstructions, using the algorithm described in [2]. Only sensors at the four standard levels up to 6.4 m were used: the sensors at 10.4 m were in too restricted an area to

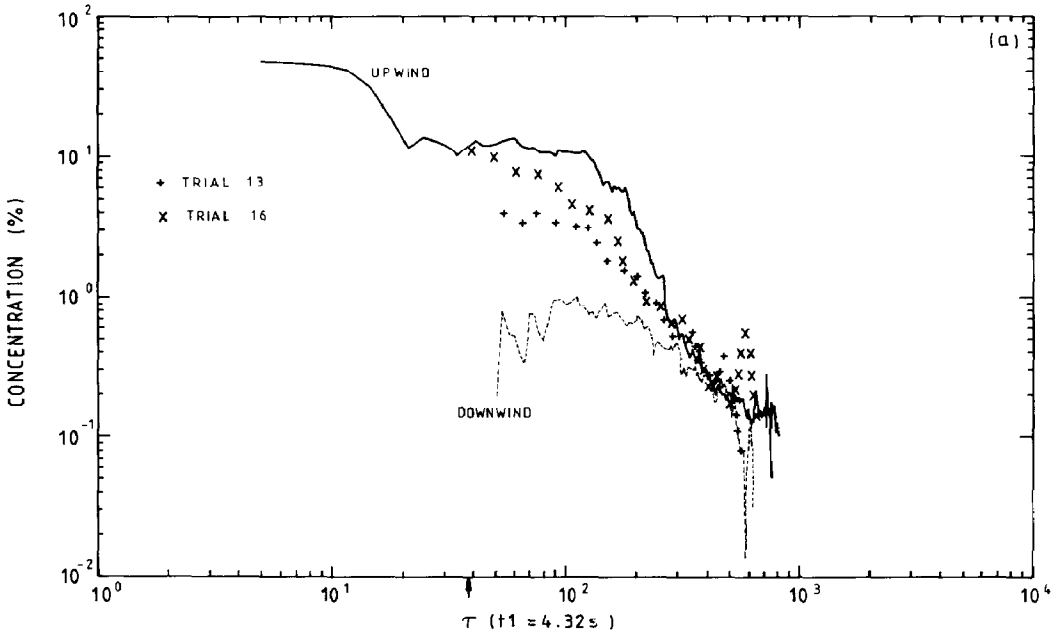

Fig. 9. Phase II barrier trials at low Richardson number: comparison of upwind and downwind area-averaged ground-level concentrations with Phase-I trials at similar Ri_0, as functions of dimensionless time τ (see Section 1.2 for definitions of τ and t_1). The arrow on the abscissa indicates the approximate time of arrival of the cloud front at the obstacle. (a) Trial 20, $Ri_0 = 500$ – 5 m fence.

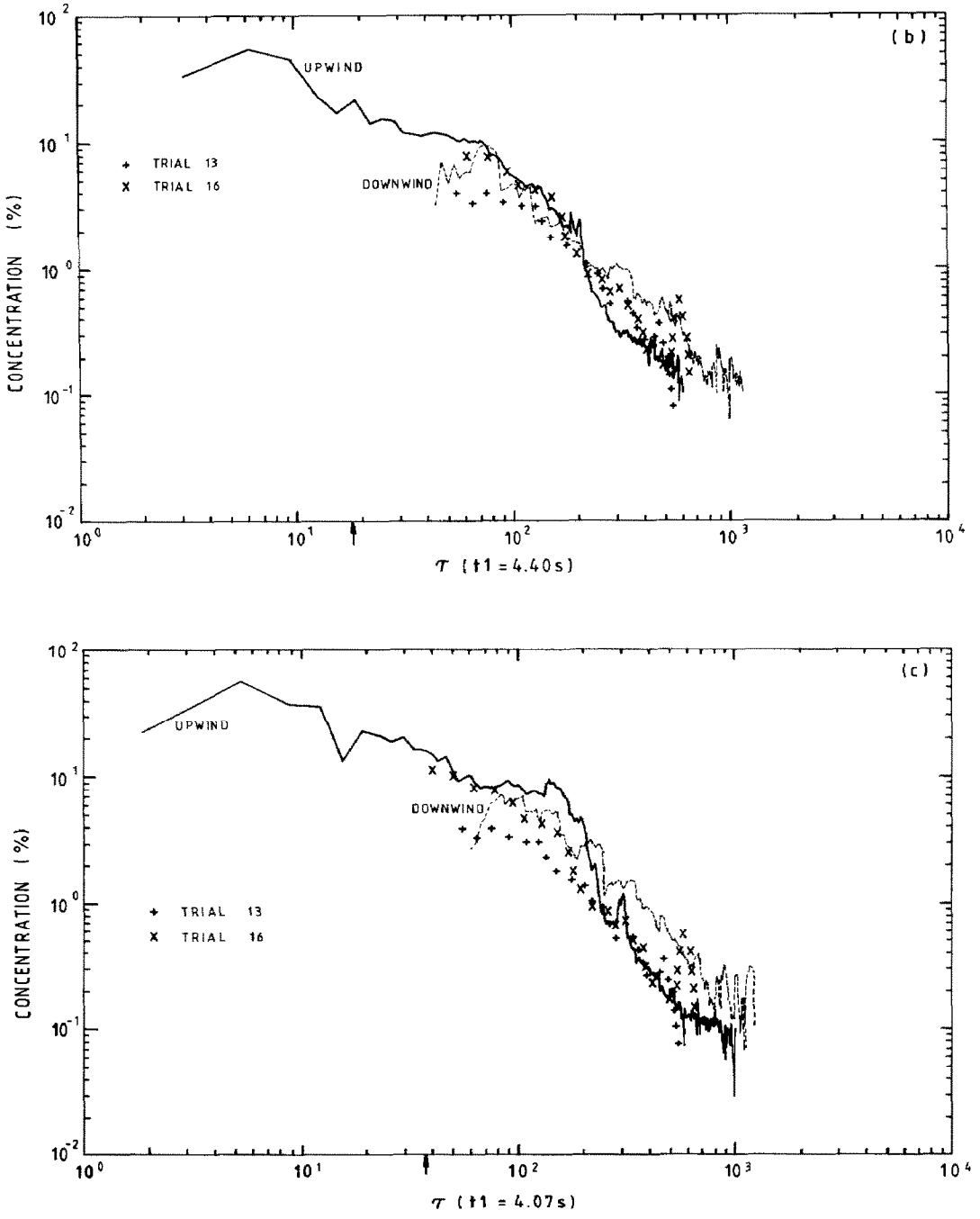

Fig. 9 (continued). (b) Trial 23, $Ri_0=535$ - 2 permeable 10 m screens. (c) Trial 24, $Ri_0=574$ - 4 permeable 10 m screens.

give representative averages, and indeed were intended to detect local effects in flow over the obstructions.

Figure 10 gives the results for Trials 20, 23, 24. The quantity plotted is an estimate of the level at which the area-averaged concentration reaches 10% of its ground-level value. It is obtained by fitting a Gaussian curve (or Gaussian with a constant portion near the ground) to the data at each one-second interval. In Trial 20 (Fig. 10(a)), the upwind height remains constant at about 4 m. Presumably this is determined directly by the fence height as at higher levels gas is rapidly removed by the wind. Downwind, the estimated height-scale rapidly becomes greater than 10 m. This means that the concentration is essentially uniform up to 6.4 m, which is the maximum height actually used for profile-fitting. The cloud is distinctly deeper than its Phase I counterparts in Trials 13 and 16. At late times downwind heights decrease again, but this is only because gas can no longer be detected at the higher levels.

In Trials 23 and 24 with the permeable screens (Figs. 10(b) and 10(c)) the upwind cloud height is again fairly constant at about 3–3.5 m, but much lower than the obstacle. Downwind the height-scales are in both cases very similar to Trials 13 and 16 and are increased by vertical mixing considerably beyond the upwind values. There is no sign of the derease in height observed by Rott-

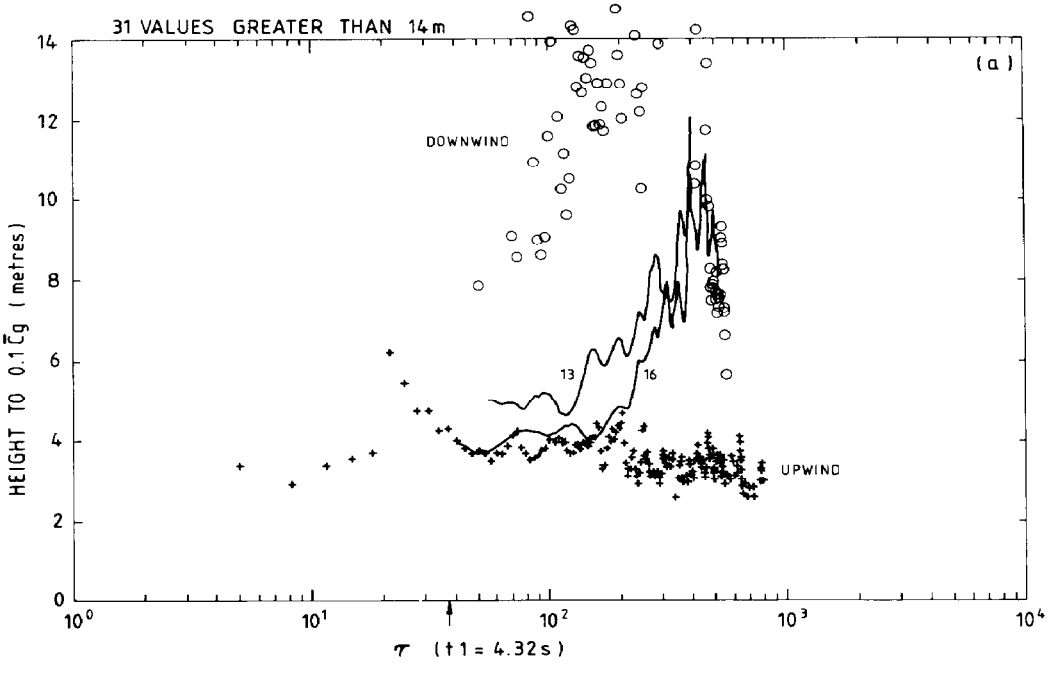

Fig. 10. As Fig. 9, but for estimated heights to 10% of area-averaged ground-level concentration. Here the continuous lines refer to the Phase I trials in similar conditions.

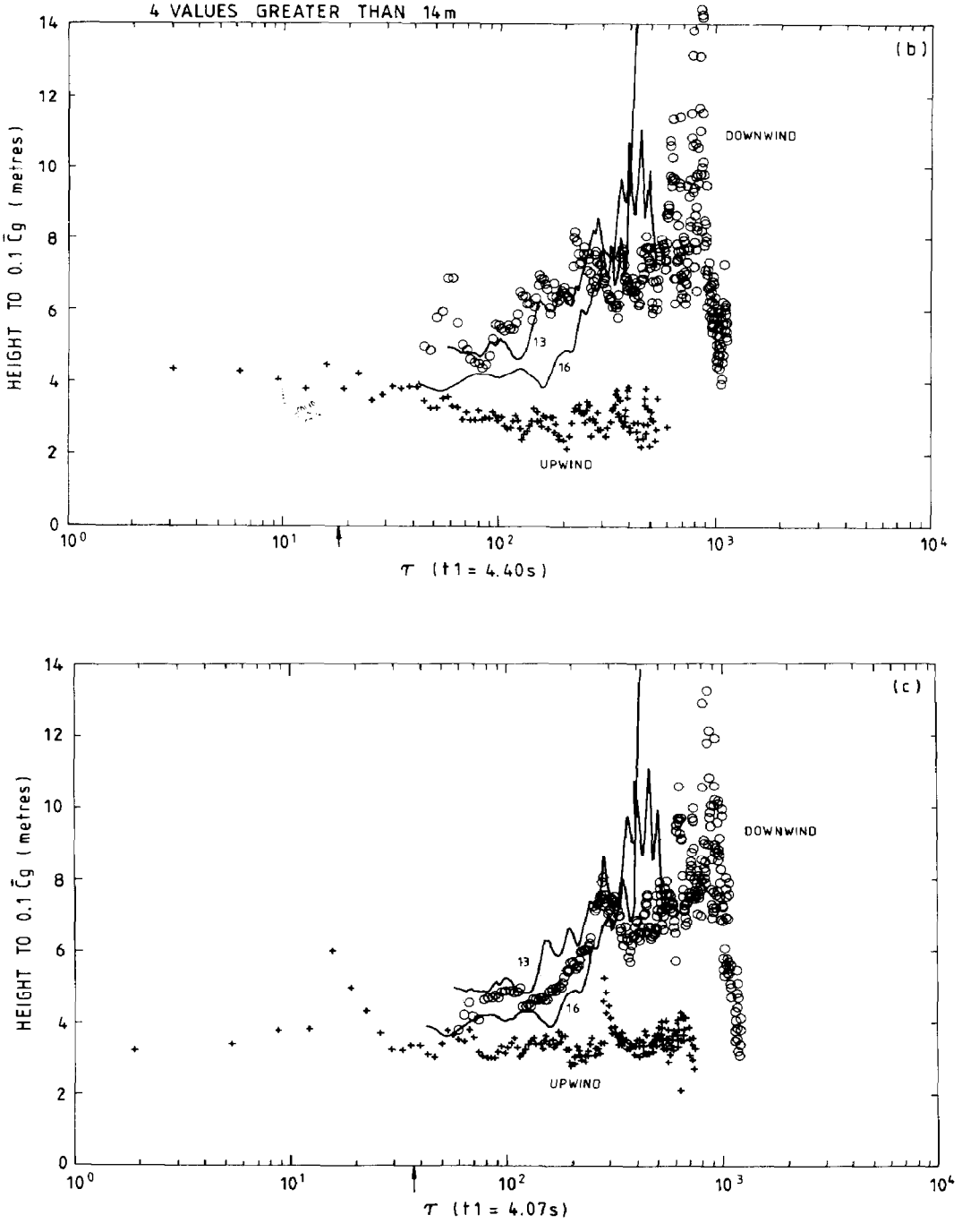

Fig. 10 (continued).

man et al. [9] when a gravity current propagates through a porous obstacle. This is perhaps because there was no ambient wind in their experiment, and particularly no turbulence in the obstacle wake.

The lack of a dramatic difference between Trial 24 and the flat-ground trials contrasts somewhat with McQuaid and Roebuck's [13] comparison of individual sensor records. At 25 m downwind they found similar peak concentrations but a much greater persistence of gas (Fig. 21.1 of [13]). Hartwig et al. [15] obtained a similar result in Trial 23 at 140 m downwind, but at 100 m the effect was not very noticeable.

As noted above, this persistene is reflected in our results not in the concentration graphs of Fig. 9 but in the movement of the centre of curvature of the clouds trailing edge listed in Table 4. McQuaid and Roebuck (Fig. 21.2) also found that the vertical scale of the cloud just downwind of the barrier in Trial 24 was much greater than in Phase I – this then seems to be a local effect since it is not reflected in our area-averaged results. The same effect was noted (Fig. 21.10 of [13], Figs. 15 and 16 of [14]) from gas sensors mounted on one of the porous screens (data from these sensors was collected separately and is not included in the standard data set).

Figure 21.5 of [13] and Fig. 17 of [14] are graphs of peak concentration against distance from the source showing a significant reduction in the far-field in Trials 23 and 24 compared to Phase I. Hartwig et al. [15] provide yet another form of presentation by calculating the mean concentration at a sensor over the period that the reading exceeds a threshold of 0.1%. Plotted against distance, this quantity is again lower for the trials with the permeable barrier than for comparable flat-ground trials but Trial 20 does not give a significant difference from flat-ground. All these apparent divergences from our results in Figs. 9(b) and 9(c) stem from the reduced overall speed of the cloud in the presence of the obstacle, this affects the different methods of analysing the concentration field in different ways.

High-Richardson-number cases

Figure 11 shows the concentration results for Trials 21, 22, 25 which had initial Richardson numbers Ri_0 of 1801, 2234 and 5275, respectively. The first two are both comparable with the flat-ground Trials 8 ($Ri_0 = 1630$) and 17 ($Ri_0 = 1860$). In Trials 21 and 22 the wind direction was within 10° of the axis of the sensor array. The results are very similar for the two trials. Upwind concentrations remain definitely higher than in the flat-ground trials until a late stage when they drop rapidly and come closer. Downwind concentrations are an order of magnitude smaller initially though this difference decreases at later times when a larger proportion of the cloud has been carried over the fence.

For individual sensor records (Fig. 21.1 of [13]) upwind sensors show similar peak values but a much more persistent signal than their Phase I counter-

parts. Plots of peak concentrations against distance from the source in Fig. 21.4 of [13] and Fig. 5 of [14] show similar reductions compared to flat-ground releases as do our area-averaged results.

Trial 25 was a low windspead case in which it was hoped that the cloud would be completely blocked by the fence. Unfortunately the wind direction was away from the sensor array and so the main cloud was not obstructed by the fence. Some gas concentrations were recorded from a part of the cloud spreading upwind beyond the fence, presumably having flowed around the end of the fence. The results in Fig. 11(c) do not have the same significance as those for Trials 21 and 22, but are remarkably similar – a matter of coincidence no doubt – the concentrations inside the fence are somewhat higher than a matching Phase I case, and those outside are about an order of magnitude smaller.

The cloud height results are given in Fig. 12. In Trial 21 the upwind height is somewhat larger than in Trial 22, which according to [14] is because of the larger initial density in the second case. There is not any clear evidence of the reflected wave seen in Davies and Singh's wind-tunnel simulation of Trial 22 ([14], Fig. 6) and predicted from shallow-layer theory [9]. The upwind height is comparable to that in Trials 8 and 17 initially, but does not increase later. Downwind, the gas has to be swept over the fence and it is expected to mix to at least the depth of the obstruction [8]. The estimated heights soon become

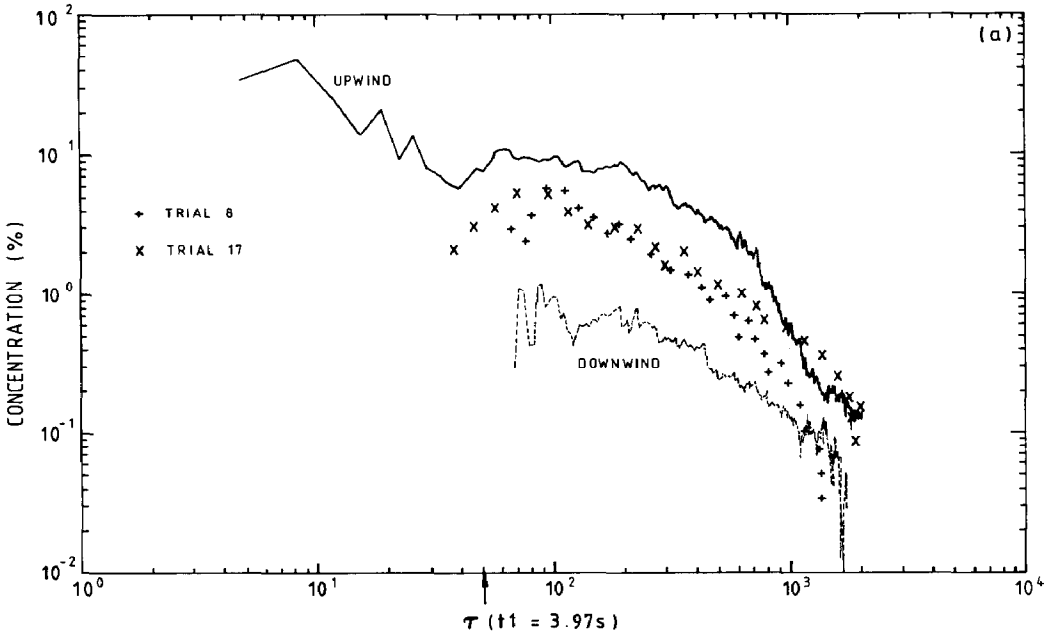

Fig. 11. As Fig. 9, for Phase-II barrier trials at high Richardson number. (a) Trial 21. (b) Trial 22. (c) Trial 25. All with 5 m fence.

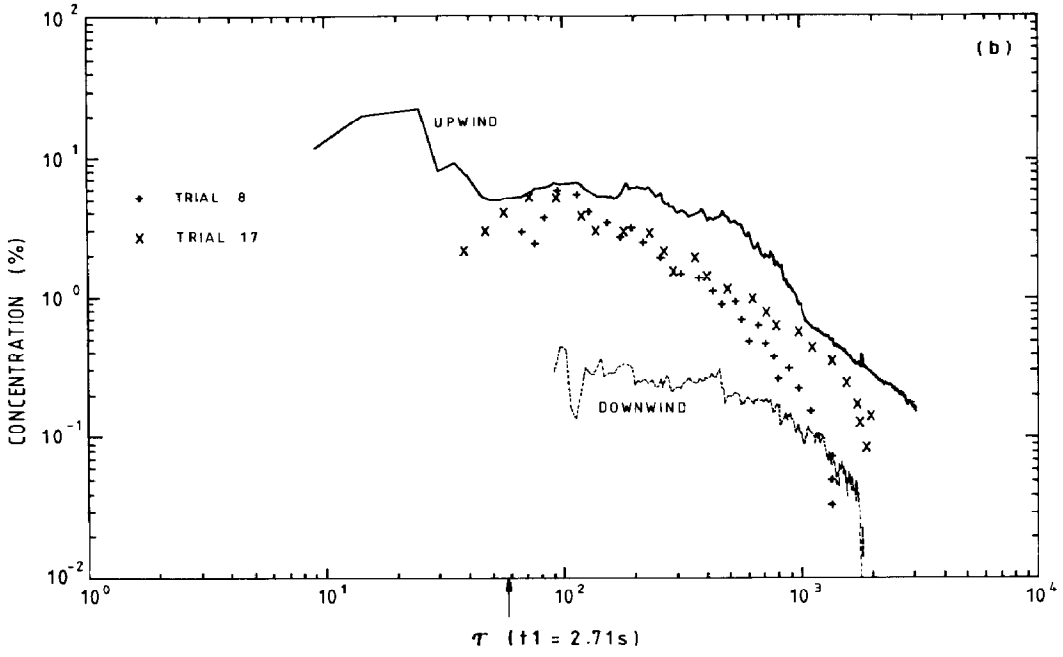
(b)
UPWIND
TRIAL 8
TRIAL 17
DOWNWIND
CONCENTRATION (%)
10^2
10^1
10^0
10^{-1}
10^{-2}
10^0
10^1
10^2
10^3
10^4
τ (t1 = 2.71s)

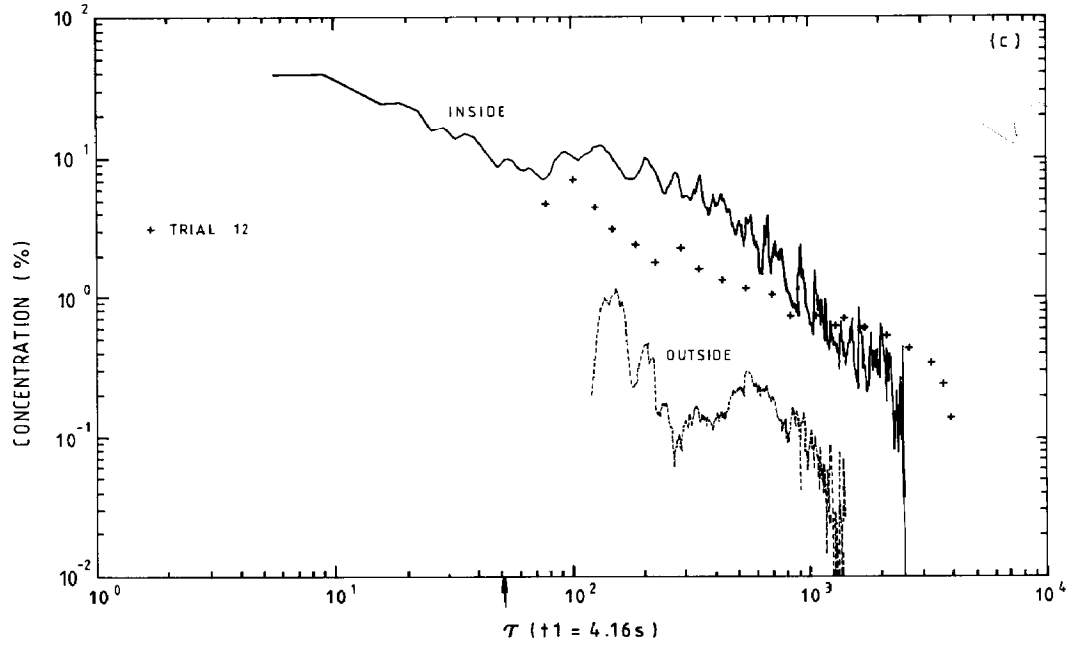
(c)
INSIDE
TRIAL 12
OUTSIDE
CONCENTRATION (%)
10^2
10^1
10^0
10^{-1}
10^{-2}
10^0
10^1
10^2
10^3
10^4
τ (t1 = 4.16s)

considerably larger than the maximum sensor height used (6.4 m) indicating a fairly uniform profile over that depth. Again the subsequent drop in the results is due to the limits of resolution at higher levels.

In Trial 25 (Fig. 12(c)), the heights outside the barrier are not increased to the same degree as in Trials 21 and 22, supporting the suggestion that the gas flowed around the end, probably suffering some enhanced turbulent mixing on the way.

5. Summing up

In this paper, we have tried to present a comprehensive account of the bulk properties of the heavy-gas clouds in Phase II of the Thorney Island trials. This is mainly intended to illuminate what went on in these particular trials, and gives an alternative perspective to comparisons based on individual sensor records or on peak concentrations.

Flat-ground trials

Three flat-ground trials not covered in [1] and [2] have been analysed. Trials 6 and 34 were consistent with the behaviour of the other Phase I Trials.

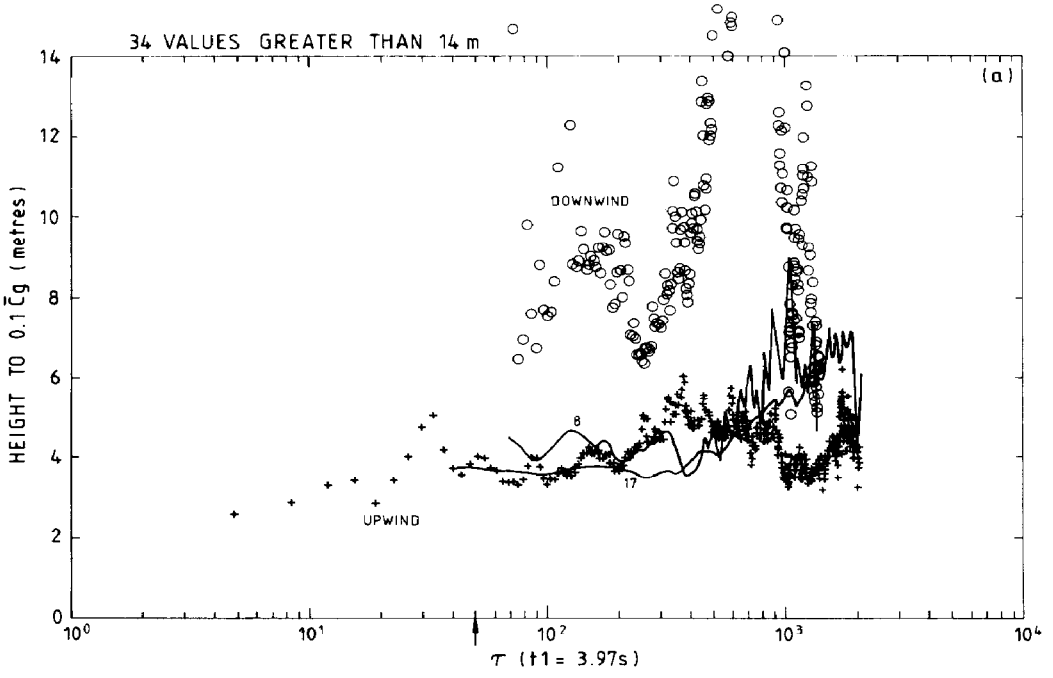

Fig. 12. As Fig. 11, but for estimated heights to 10% of area-averaged ground-level concentration. here the continuous lines refer to the Phase I trials in similar conditions.

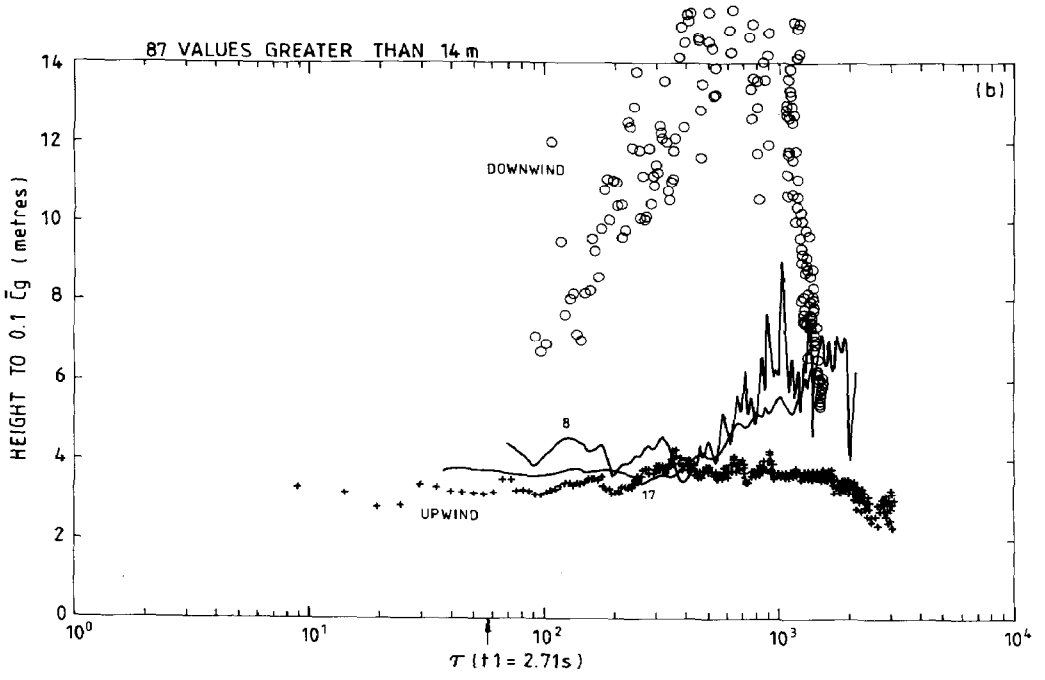
87 VALUES GREATER THAN 14 m
(b)
DOWNWIND
UPWIND
8
17
HEIGHT TO 0.1 $\bar{C}_g$ (metres)
τ (t1 = 2.71s)

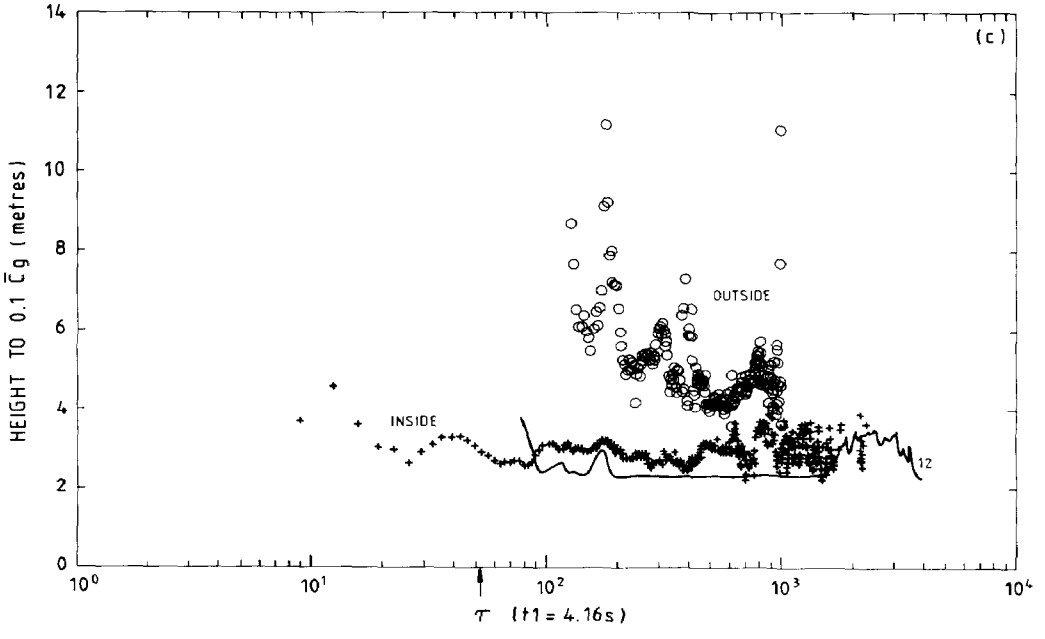
(c)
OUTSIDE
INSIDE
12
HEIGHT TO 0.1 $\bar{C}_g$ (metres)
τ (t1 = 4.16s)

Trial 5 showed considerably lower concentrations than expected from the correlation of Wheatley et al. [5,6] which describes very satisfactorily the development of concentration in Trials 7–19. One contributing factor may be atmospheric instability, but as the release was flawed and the maximum number of masts in the cloud was only 4, the discrepancy may not be significant.

Building trials

The photographic analysis could be applied to only two of the releases with the building and showed that the building has no effect on the initial gravity-spreading behaviour, up to the time the cloud front reaches the obstacle. Analysis of arrival and departure times showed that subsequent development of the overall cloud outline was not affected, though local effects near the building can not be resolved by the method. This conclusion was not surprising since the building with a side of length 9 m was very small compared to a cloud several hundred metres in extent. However, analysis of mean cloud concentrations gave results which in some cases were significantly smaller than Wheatley et al.'s [5,6] correlation. The most glaring example, Trial 26, was associated with unusually unstable atmospheric conditions, and it appears that the correlation of Wheatley et al. may need modification in such conditions (which are outside the range of the data on which it was based). It is possible that building-wake turbulence may also have been a contributory factor despite the small size of the obstacle.

Local effects near the building have also been examined. The most striking feature was the reduction of concentration by up to an order of magnitude on the front face of the obstacle. This is probably due to the existence of a horseshoe vortex wrapped round the upwind faces of the building (see Hunt et al. [20], Fig. 15 for a good illustration). This would tend to bring air from a higher level down the faces of the building and outwards at ground-level, opposing the approach of heavy gas at ground level. In the near-wake of the building with its recirculatory, highly turbulent flow, there were not any very marked effects on concentrations compared to the overall cloud average. A similar effect of a horseshoe vortex has been observed by Krogstad and Pettersen [21] in wind-tunnel experiments on a continuous heavy-gas plume encountering a cuboidal obstacle. However, they also found that concentrations in the near-wake were reduced by similar amounts to those upwind.

Barrier trials

The semi-circular fence and permeable screens presented a much more severe obstacle than the building because the whole cloud had to pass over or through them. Right up to the time that the cloud front reaches the barrier, there is no effect on the gravity-spreading rate but the translational advection speed is considerably smaller than on flat ground. The next stage in which the heavy gas splashes over the fence and a reflected wave may be observed has been

described by other authors [9,13,14]. Our studies indicate the subsequent overall behaviour of the cloud. Part of the cloud is trapped upwind of the barrier in a virtually stagnant region, with the wind carrying material slowly over the top. Downwind the cloud is much deeper and more dilute than in corresponding flat-ground cases, but the leading part is advected downwind at much the same speed. The effect of the reduction in windspeed in the wake of the obstacle must be counterbalanced by the greater cloud height. The cloud downwind tends to spread at a slower rate beause of its depleted buoyancy content. Unfortunately, it does not seem possible to estimate how rapidly material is transferred from the upwind to downwind parts of the cloud: the cloud area upwind cannot be determined, nor the cloud height downwind. At late times, mean concentration in the downwind part of the cloud approach those in flat-ground trials in equivalent conditions.

The above description applies to the impermeable fence. With the permeable screens, effects are less severe. Local measurements indicate that the cloud depth is increased within the obstacle [13,14]. Downwind, average cloud height and concentration are about the same as over flat ground (as functions of time). The speed of the front is little affected. There is however a distinct reduction in the speed of the rear of the cloud, which as a result becomes more elongated and grows in area more slowly than over flat ground.

Acknowledgement

This work has been carried out for the U.K. Health and Safety Executive.

References

1 P.W.M. Brighton, A.J. Prince and D.M. Webber, Determination of cloud area and path from visual and concentration records, J. Hazardous Materials, 11 (1985) 155-178.
2 P.W.M. Brighton, Area-averaged concentrations, height-scales and mass balances, J. Hazardous Materials, 11 (1985) 189-208.
3 A.J. Prince, D.M. Webber and P.W.M. Brighton, Thorney Island Heavy Gas Dispersion Trials - determination of path and area of cloud from photographs, UKAEA Report SRD R318, 1985.
4 P.W.M. Brighton, Using concentration data to track clouds in the Thorney Island experiments, UKAEA Report SRD R319, 1986.
5 C.J. Wheatley, A.J. Prince and P.W.M. Brighton, Comparison between data from the Thorney Island Heavy Gas Trials and predictions of simple dispersion models, UKAEA Report SRD R355, 1986.
6 C.J. Wheatley, P.W.M. Brighton and A.J. Prince, Comparison between data from the heavy gas dispersion experiments at Thorney Island and predictions of simple models, In: C. de Wispelaere (Ed.), Air Pollution Modelling and its Application V, Plenum, New York, 1986, pp. 717-731.
7 C.J. Wheatley and A.J. Prince, Translational cloud speeds in the Thorney Island trials: mathematical modelling and data analysis, J. Hazardous Materials, 16 (1987) 185-199.

8 R.E. Britter, Special topics on dispersion of dense gases, Report on Contract No. 1200/01.01, Research and Laboratory Services Division, HSE, Sheffield, 1982.
9 J.W. Rottman, J.E. Simpson, J.C.R. Hunt and R.E. Britter, Unsteady gravity current flows over obstacles: some observations and analysis related to the Phase II trials, J. Hazardous Materials, 11 (1985) 325–340.
10 Health and Safety Executive, Heavy Gas Dispersion Trials: Data Books, Research and Laboratory Services Division, Broad Lane, Sheffield S3 7HQ, 1982–83.
11 T.O. Spicer and J.A. Havens, Modelling the Phase I Thorney Island experiments, J. Hazardous Materials, 11 (1985) 237–260.
12 D.G. Beesley, Unpublished SRD memoranda, 1984–85.
13 J. McQuaid and B. Roebuck, Large scale field trials on dense vapour dispersion, Report EUR 10029, Commission of the European Communities, Brussels, 1985.
14 M.E. Davies and S. Singh, The Phase II trials: a data set on the effect of obstructions, J. Hazardous Materials, 11 (1985) 301–323.
15 S. Hartwig, W. Heudorfer and G. Schnatz, Dynamic behaviour of a heavy gas cloud in the presence of an obstacle, presented at the Symposium on Heavy Gas Dispersion Trials at Thorney Island — 2, Sheffield, Great Britain, September 1986.
16 P.W.M. Brighton, A user's critique of the Thorney Island dataset, J. Hazardous Material, 16 (1987) 457–500.
17 J. McQuaid, Objectives and design of the Phase I Heavy Gas Dispersion Trials, J. Hazardous Materials 11 (1985) 1–33.
18 M.E. Davies and S. Singh, Thorney Island: its geography and meteorology, J. Hazardous Materials, 11 (1985) 91–124.
19 J.S. Puttock, Analysis of meteorological data for the Thorney Island Phase I trials, J. Hazardous Materials, 43–74.
20 J.C.R. Hunt, C.J. Abell, J.A. Peterka and H. Woo, Kinematical studies of the flows around free or surface-mounted obstacles; applying topology to flow visualizationn, J. Fluid Mech., 86 (1978) 179–200.
21 P.Å. Krogstad and R.M. Pettersen, Windtunnel modelling of a release of a heavy gas near a building, Atmos. Environ., 20 (1986) 867–878.